DETECTION AND ANALYSIS OF SOFT NANOPARTICLES

BY THE RESISTIVE PULSE METHOD

by

Deric Avery Holden

A dissertation submitted to the faculty of
The University of Utah
in partial fulfillment of the requirements for the degree of

Doctor of Philosophy

Department of Chemistry

The University of Utah

August 2012

STATEMENT OF DISSERTATION APPROVAL

The dissertation of **Deric Avery Holden**

has been approved by the following supervisory committee members:

Henry S. White	, Chair	**July 13, 2012** Date Approved
Joel M. Harris	, Member	**July 13, 2012** Date Approved
Marc D. Porter	, Member	**July 13, 2012** Date Approved
Michael D. Morse	, Member	**July 13, 2012** Date Approved
Richard B. Brown	, Member	**July 13, 2012** Date Approved

and by **Henry S. White** , Chair of

the Department of **Chemistry**

and by Charles A. Wight, Dean of The Graduate School.

ABSTRACT

Soft nanoparticles have become increasingly important to the scientific and medical communities particularly in drug delivery systems due to their ability to deliver drugs in a time-dependent or site-specific manner. However, much is left unexplored in their permeation and translocation through porous biological membranes, such as those found in the body. This dissertation presents investigations of the resistive-pulse detection and analysis of soft nanoparticles including microgels and liposomes, using conical nanopores embedded in glass membranes. This analysis provides a first look at the permeation and translocation of soft nanoparticles through a porous membrane. Chapter 1 overviews nanoparticles and their uses in the scientific and medical communities, as well as the resistive-pulse technique and the glass nanopore membrane.

Chapter 2 describes investigations on the pressure dependent deformation and translocation of 570 nm radius pNIPAm-AAc microgels through small conical nanopores in glass membranes using the resistive-pulse technique. Translocation event rates, durations, and current pulse heights are found to be a function of the relative conductivities of the microgel and the electrolyte solution. Also, a statistical analysis technique is used to determine the probability of coincident events.

Chapter 3 presents experimental results on the deformation and dehydration of the 570 nm radius microgels through the glass nanopore membrane through smaller pore while under pressure. A translocation threshold pressure is observed and measured as a function of the pore size. Current-time traces are also investigated and provide insight into the microgels ability to both deform and dehydrate while undergoing translocation.

Chapter 4 reports the temperature dependent translocation of 190 to 450 nm radius liposomes through the glass nanopore membrane both above and below the liposome's lipid bilayer transition temperature. Liposomes at or below their bilayer transition temperature behave rigidly and are captured at the nanopore orifice while attempting to translocate through pores of smaller dimensions. Liposomes above their transition temperature are capable of deformation and translocation through nanopores that are smaller than the liposome radius. The evolution from soft to hard liposomes was monitored as a function of the temperature while the liposome underwent translocation through a nanopore of smaller dimensions.

CONTENTS

LIST OF ABBREVIATIONS

℃ – degree Celsius

2-D – 2 dimensional

Å – Angstroms

AAc – acrylic acid

Ag/AgCl – silver/silver chloride

Cl^- – chloride ions

cm – centimeters

COOH – carboxylic acid

DLPC – 1,2-dilauroyl-*sn*-glycero-3-phosphocholine

DLS – dynamic light scattering

DNA – deoxyribonucleic acid

DOPS – 1,2-dioleoyl-*sn*-glycero-3-phospho-L-serine (sodium salt)

DPPC – 1,2-dipalmitoyl-sn-glycero-3-phosphocholine

DPPG – 1,2-dipalmitoyl-*sn*-glycero-3-phospho-(1'-*rac*-glycerol) (sodium salt)

GNM – glass nanopore membrane

ICR – ion current rectification

i_{lim} – limiting current

i_o – open pore current

i-t – current-time

K^+ – potassium ions

K_2HPO_4 – dipotassium phosphate

KCl – potassium chloride

KH_2PO_4 – monopotassium phosphate

kHz – kilohertz

mL – milliliter

mmHg – millimeters mercury

m*V* – millivolts

MΩ – megaohm

NaCN – sodium cyanide

NaOH – sodium hydroxide

NH_2 – amine

nm – nanometers

NP – nanoparticles

P – pressure

P_{min} – minimum pressure

pNIPAm-AAc – poly(*N*-isopropylacrylamide-*co*-acrylic acid)

PS – polystyrene

Pt – platinum

Q – Volumetric Flow Rate

RNA – ribonucleic acid

R_{pore} – radius of nanopore

$R_{\mu gel}$ – radius of microgel

T – temperature

T_c – lipid bilayer transition temperature

V – voltage

V – volts

Δi – current deviation

Δt – translocation time

μgel – microgel

μm – micrometers

μs – microseconds

ACKNOWLEDGEMENTS

I would like to acknowledge and thank my advisor Dr. Henry S. White for his contributions during my graduate career. His knowledge, guidance, and patience have been vital to the completion of this dissertation. I consider myself fortunate to have been able to work with him and am hopefully a better scientist because of it.

I would like to thank a number of people who also contributed to my success and helped me in immeasurable ways in this research. In particular I would like to thank Dr. Wenjie Lan, Mr. Grant R. Hendrickson, Dr. L. Andrew Lyon, Dr. Anna Schibel, Ms. Qian Jin, Mr. Jiewen Xiong, Mr. Long Luo, Ms. Jessica Egan, Mr. Nils Bauman, Dr. Peter Birkin, Mr. Ron Jones, and Dr. John J. Watkins.

Finally, I would also like to sincerely thank my family, especially my wife Korin, for their love, support, and encouragement.

CHAPTER 1

INTRODUCTION

1.1 Soft Nanoparticles

This dissertation describes the detection and analysis of soft, flexible nano-scale particles using the glass nanopore membrane (GNM) and the resistive-pulse technique. Recently, nanoparticles, including soft nanoparticles, have been studied and developed by the scientific and medical communities for drug transport and delivery applications,[1-5] cancer treatment,[6,7] and other biological processes[8-13] due to their ability for site-specific and time-released delivery. Traditional delivery of pharmaceutics into the body relied on the circulatory system and often resulted in the delivery of drugs to undesired locations or at unwanted concentrations owing to the inability to control the permeation of the drugs in the body.[8,12-14] These problems are being addressed with the development of new delivery methods including the use of nanoparticles for site-specific or time-released pharmaceutics. Various types of soft nanoparticles, including liposomes[5] and biodegradable polymeric nanoparticles made from substituents such as polyesters,[15-17] facilitate the dispersion and permeation of pharmaceutics throughout the body due to their ability to bind both drugs and recognition markers to a single nanoparticle and deliver it via intravascular, pulmonary, subcutaneous, or oral routes.[18] Additionally, many

types of soft nanoparticles, including liposomes, have the ability to release drugs at a constant concentration over a long duration. Despite the role that nanoparticles are now playing in drug delivery systems, much is left to be investigated in the processes that surround their permeation through the body. This dissertation describes fundamental studies on various types of soft nanoparticles, including microgels and liposomes, as they translocate through porous membranes with pore dimensions similar to or smaller than the nanoparticles themselves. This dissertation provides vital information about the nature of the nanoparticles as they encounter biological membranes. Information gained in these experiments may help optimize the use of soft nanoparticles as a platform for drug delivery.

Nanoparticles are often defined as objects or particles with dimensions on the nanometer scale. They may exhibit physical, optical, electronic, or chemical properties that are different from the corresponding bulk materials.[14] For example, gold nanoparticles absorb blue light while they scatter red light giving gold nanoparticles a deep red color as opposed to the bulk gold color so well known. Additionally, due to their small size, nanoparticles have a large surface area to volume ratio. If a 1 x 1 x 1 cm solid sample is broken up into 100 x 100 x 100 nm particles, it would have 1 x 10^{15} times more surface area than the original sample. This is often important in many analytical or medical applications including site-specific drug delivery where a large, modifiable surface area in a small volume is needed.[1,10,14,19,20]

Some of the first few experiments involving detection of particles in the nano-regime were performed by Granqvist and Buhrman in the 1970s when they measured the absorption spectrum of ultrafine aluminum particles smaller than 10 nm[21] and by DeBlois et al. when they detected nano-scale viruses, including type C oncornaviruses, using the resistive-pulse technique.[22,23] Since that time many chemical, optical, and physical properties of nanoparticles have been explored producing a variety of nanoparticles useful in a wide range of fields ranging from fundamental science, to new materials, medical diagnostic tools and drug delivery systems.[14]

Some of the more common types of nanoparticles currently used in scientific research include metallic nanoparticles,[2] polystyrene or other polymer-based nanoparticles,[19,20] and magnetic nanoparticles.[24-26] These highly uniform, inflexible particles are typically formed from either the reduction of metal ions (e.g. gold nanoparticles formed from the reduction of chloroauric acid), or grown from organic precursors (e.g. polystyrene nanoparticles formed from styrene monomers). Additionally, many nanoparticles contain surface modifications terminating in either carboxylic acids (COOH) or primary amines (NH_2) yielding particles with pH dependent properties and capable of binding to proteins,[27-29] antibodies,[30] DNA and RNA,[31,32] polymers,[33] and viruses[22,23,34] or other biologically reactive ligands creating a highly reactive surface. These modified hard nanoparticles are useful for various types of analytical or biological procedures and are of particular interest in drug delivery systems due to their ability to bind multiple drug moieties and recognition sites to a single particle. As

such, several of commercial companies, such as Bangs Laboratories and Ted Pella, Inc., sell hard particles with COOH and NH_2 surface modifications, or with protein coupling kits.[35,36]

A major disadvantage, however, of using particles is their toxicity in the human body.[8,12-14] Metal ions from gold, silver, and iron can disrupt or alter many of the body's biological processes creating complications such as blood clotting, thrombosis, cardiovascular malfunction and cytotoxicity of the liver and kidneys.[12,14] Additionally, large nanoparticles (>100 nm) are preferentially taken up by the liver, spleen, and lungs quickly reducing their effectiveness, while small nanoparticles are toxic to cells.[12,37]

In contrast, soft, flexible particles overcome some of the disadvantages presented by hard particles, and are thus being proposed for and used in drug delivery systems.[3,4,38-44] Unlike their hard counterparts, soft particles have the advantage of being flexible and are not absorbed by the mononuclear phagocyte system and thus circulate through the body for longer periods of time compared to hard particles of the same size.[12,37] Many have the additional advantage of being porous or multilayered, with the ability to store hydrophobic or hydrophilic compounds, readily available for transport and delivery to various parts of the body.[5,38,39] Finally, these soft nanoparticles are often made from biologically friendly constituents like lipid bilayers, forming vesicles or liposomes,[3,4,38,39] or loosely-bound polymers, such as combinations of acrylic acid and *N*-isopropylacrylamide residues, forming hydrogels and microgels and are able to

break down and decompose inside the body eliminating unwanted concentration build-ups. [5,38-44]

This dissertation presents investigations of the translocation of microgels and liposomes through a nanopore, particularly where particle deformation is required. Both of these soft nanoparticles are relevant to the medical community as site-specific transport vehicles for pharmaceutics.

1.2 The Resistive-Pulse Technique

Many methods currently exist for determining the size, shape, and charge of nanoparticles. The most common characterization methods are light scattering,[45,46] electron microscopy,[47-49] optical microscopy,[50-52] and the resistive-pulse technique.[53] While each has its own distinct advantage in the scientific community, this dissertation focuses on the resistive-pulse technique and its ability to detect and analyze the translocation of soft nanoparticles through a porous membrane.

The resistive-pulse technique began with the work of Wallace H. Coulter in 1953.[53] In that pioneering work, a single channel separated two electrolyte filled reservoirs. Particles were driven from one reservoir through the channel and into the second by applying a small pressure to one side of the membrane. Electrodes placed on opposing sides of the membrane generated a voltage across the channel, and a sensing zone formed at the tightest portion of the channel where the greatest potential drop occurs. As a particle passed through the channel, it excluded the electrolyte solution, momentarily decreasing the ionic conductance through the pore and the measured current, giving rise to a

resistive-pulse. Today, modern resistive-pulse techniques use the same basic concepts developed over 50 years ago. Using the resistive-pulse method, a particle's translocation through a porous membrane is able to be monitored and better understood. The resistive-pulse method results in change in the pore's resistance proportional to the particle size, and duration related to the charge, size, and mobility of the particle.[54] The event rate, measured in the number of events per unit time, is proportional to the particle concentration.[31] Furthermore, because translocation events occur stochastically, statistical methods can be used to obtain averages, distributions, and likelihood of two events occurring simultaneously.[55-57]

Originally, the Coulter-Counter was developed to measure cells and bacteria with pores around 100 μm, but these same pores were incapable of measuring nanoparticles due to the small amount of electrolyte displaced by the nanoparticle in the sensing zone during translocation.[53] In practice, particles with diameters smaller than ~1/3 of the pore create changes in the current too small to be detected above the background noise.[58] In the past decade, however, the Coulter-Counter and the resistive-pulse technique have progressed rapidly from the micoscale to the nanoscale, resulting in a variety of adaptations and can now detect nanoparticles down to a few nanometers.[31,32,58-61]

Many of the channels currently used in the resistive-pulse method may be cylindrical,[22,23,62-69] while others are conical[55,58,70-75] like that in Figure 1.1, where a schematic of the resistive-pulse technique using pressure and voltage to drive particles through a conical channel between two reservoirs is shown. The current

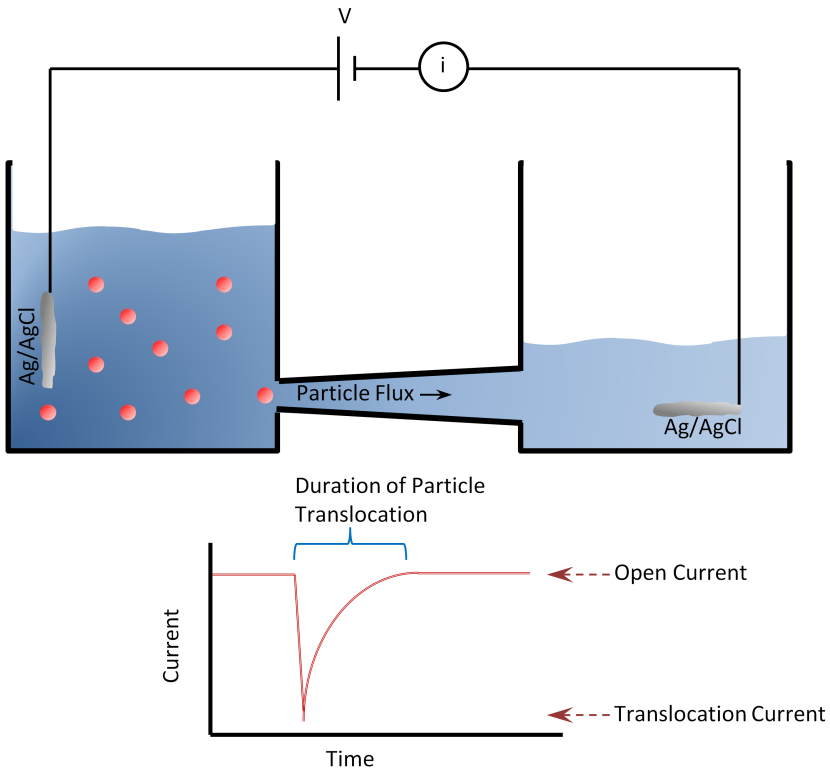

Figure 1.1 A schematic diagram depicting a resistive-pulse setup through a conical nanopore separating two reservoirs. A hydrostatic pressure is applied via a solution height difference in the two reservoirs driving the particles from the left to the right reservoirs through the nanopore. The particle translocation is monitored by measuring the change in current through the pore generated by a potential difference between two Ag/AgCl electrodes.

is measured as a function of time and decreases whenever a particle moves through the pore. The resulting current-time signature is a product of the particle and channel geometries as the particle moves through the portion of the pore where the electric field is the greatest. For instance, a particle moving from left to right through the conical pore in Figure 1.1 creates a sharp decrease in conductivity as it first encounters the small orifice of the pore, where the electric field is strongest. Then, as the particle proceeds through the pore it quickly occupies less of the volume where the electric field is strongest, returning the current to the original open-pore level. This gives rise to an asymmetrical pulse like that shown in Figure 1.1. The reverse pulse is observed if the particle moves from right to left.

One advantage to using conical pores includes localizing the electric field and sensing zone at the small orifice, thereby detecting only one particle at a time. However, this often results in strong electrophoretic forces acting on the particles causing fast translocation times and events often too short for current electronic instrumentation to adequately measure without some distortion.[55,58,70-75] Cylindrical pores, on the other hand, distribute the potential drop, and thus the sensing zone, across the entire length of the pore evenly allowing the particle to be detected and analyzed during the entire duration of the translocation event.[22,23,62-69] However, because the sensing zone is spread out over a large length, more than one particle may be in the sensing zone at any time, giving rise to large complicated events. Ultimately, the geometry used in a resistive-pulse

experiment is decided by the objective of the experiment, the capabilities of the instrumentation, and the fabrication technique of the pore.

Currently, nanopores are synthesized in membranes of silicon nitride, PDMS, sapphire, Al_2O_3, glass, or made with single- or multi-walled carbon nanotubes or biological pores such as α-hemolysin or mycobacterial porins.[31,32,54,58-77] Typically, the membrane material is chosen because of the fabrication technique or some desired characteristics of the system such as noise levels,[78-81] ease of fabrication,[76] tunability,[82,83] or ability to integrate with micro- and nano-fluidic systems.[84-87] For example, Willmott et al. created a pore in a thermoplastic polyurethane membrane which has a radius capable of being tuned between 500 nm and 20 μm.[82,83] This allows for the detection of particles with radii spanning over two orders of magnitude. Other groups have integrated nanopores into micro or nano-fluidic systems, which can be optimized for small volumes, and are useful when only a small sample is available.[84-89]

1.3 The Glass Nanopore Membrane

In this dissertation, a conical nanopore embedded in a glass membrane, hereafter referred to as the glass nanopore membrane (GNM), is used. The method for fabricating the GNM is well documented[76] but is briefly summarized here. First, a short length Pt wire is electrochemically sharpened and then sealed into either a borosilicate or soda-lime glass capillary. Polishing removes excess glass until a Pt disk is exposed. The disk radius, r, may be determined by measuring the diffusion limited current, i_{lim}, in a known redox solution and using the ultra-microelectrode diffusion-limited steady-state relation:

$$i_{lim} = 4nFDCr \quad (1.1)$$

where *F* is Faraday's constant, and *D, C,* and *n* are the diffusion coefficient, the concentration of the redox molecule, and the number of electrons involved in the redox process, respectively.[76,90] The Pt is then electrochemically etched out and removed from the glass membrane resulting in a small conical nanopore embedded in the end of a glass capillary. The radius, *r*, of the small orifice of the GNM is then recalculated by measuring the ionic resistance, *R*, in a 1 M KCl solution and using equation 1.2:[76]

$$R = \frac{1}{\kappa r}\left(\frac{1}{\pi \tan(\theta)} + \frac{1}{4}\right) \quad (1.2)$$

In equation 1.2, κ is the conductivity of the solution and θ is the half cone angle measured in radians. Equation 1.2 can be further simplified by estimating κ (0.1119 Ω^{-1} cm^{-1} at 25 ℃ for 1 M KCl solution) and assuming a cone angle (estimated by optical microscopy) of 10°, then rearranging to solve for *r*:

$$r = 0.185/R. \quad (1.3)$$

In equation 1.3, the constant 0.185 has units of nm·GΩ, while the degree of error involved in this estimation is estimated to be about 10% and is primarily caused by slight changes in the cone angle, θ.[76]

GNMs may be used for translocation experiments in this unmodified state, or modified in a variety of ways depending on use. Unmodified GNMs have deprotonated silanol groups at neutral pHs giving rise to a significant negative

charge on the surface of the glass and a potential and ion distribution that extend into the sensing zone. This negative charge electrostatically repels Cl^-, while attracting K^+, and the non-uniform ion distribution extends approximately a distance of $5\kappa^{-1}$ into the solution,[91,92] where κ^{-1} is the Debye screening length defined by:

$$\kappa^{-1} = \sqrt{\frac{\varepsilon_r \varepsilon_o RT}{2z^2 F^2 C}} \tag{1.4}$$

In equation 1.4, ε_r is the relative permittivity, ε_o is the permittivity in a vacuum, *R* is the gas constant, *T* is the absolute temperature, *z* is the electrolyte charge, *F* is Faraday's constant, and *C* is the bulk electrolyte concentration.

For pores that have radii on the same order as $5\kappa^{-1}$ the electric double layer overlap causes a K^+ selective zone preventing Cl^- flux through the pore. When a positive potential is applied to the interior of the pore the Cl^- is removed from the pore orifice decreasing the conductivity in the sensing zone. When a negative potential is applied, the Cl^- cannot pass through the K^+ selective zone and a concentration buildup occurs increasing the conductivity.[93-95]

This unequal ion flux at positive and negative voltages causes a deviation of the current from the expected ohmic behavior as shown in Figure 1.2 and is known as ionic current rectification (ICR). ICR was first observed by Wei et al. in 1995 using quartz nanopipets,[96] and has additionally been observed in pores made with various materials, of different sizes, and with various surface modifications.[96-100] ICR in an unmodified GNM increases current from ohmic

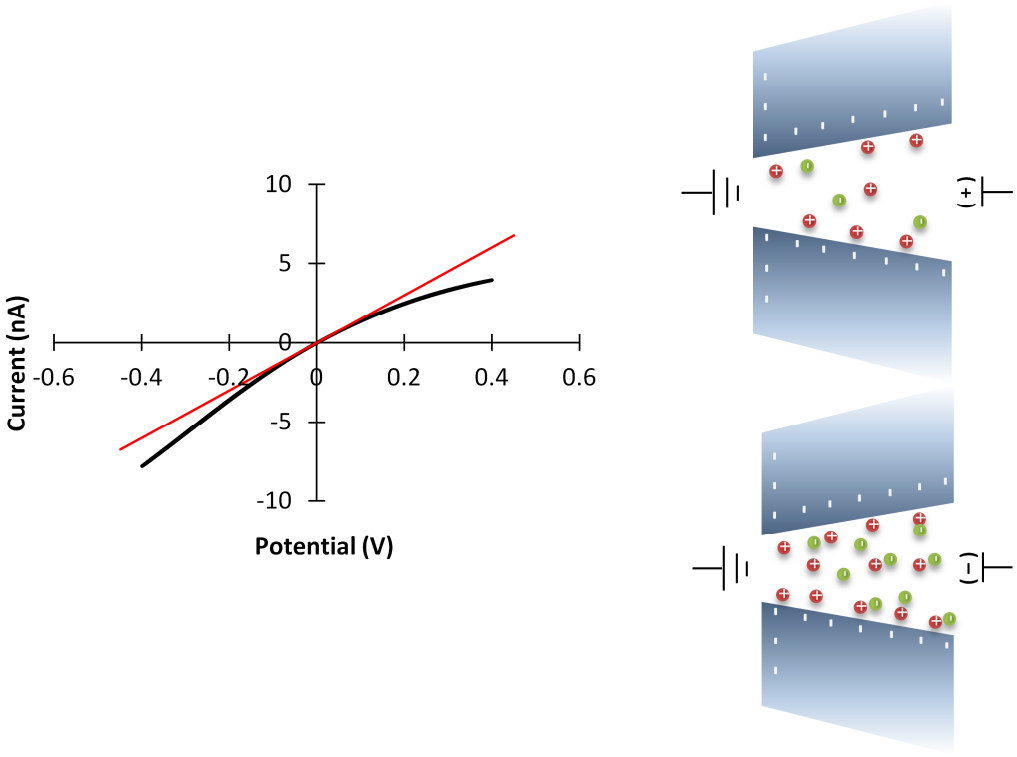

Figure 1.2 Left) *i-V* graph of a 155 nm GNM exhibiting ion current rectification in a 10 mM KCl solution. Legend – pore exhibiting ion current rectification, – pore exhibiting ohmic response. Right) Schematic representations of the ion distribution in a conical nanopore exhibiting ionic current rectification.

behavior at negative voltages (outside vs. inside) and decreases current from ohmic behavior at positive voltages (outside vs. inside).

Surface modification of GNM is typically performed by chemically reacting the exposed surface silanol groups on the glass with either 3-cyanopropyldimethylchlorosilane or trimethylchlorosilane. In this dissertation, surface modification is primarily performed to reduce or change the surface charge on the GNM from a negatively charged surface to a neutral one, thus reducing ICR, or in some circumstances to make the surface more hydrophobic.

In the case where a pressure driven translocation was expected, an analytical expression for calculating theoretical volumetric flow rates was derived from the Hagen-Poiseuille equation for volumetric flow through a capillary and adjusting for a conical geometry; the full details are explained elsewhere,[74] however, equation 1.5 shows the relation:

$$Q = \frac{3\pi r^3 P}{8\eta \cot(\theta)} \tag{1.5}$$

where Q is the volumetric flow rate of the solution, P is the pressure, η is the solution viscosity, r is the pore radius, and θ is the half cone angle. The expected event rate can then be obtained by multiplying Q, in mL/s, with the concentration, in events/mL, to get an estimated event rate, in events/s. Estimated event rates are compared against experimental data throughout this dissertation.

1.4 Finite-Element Simulations

Finite-element computer simulations have been used to model the ionic current and electric field through nanopores during particle translocation in order to better understand and predict translocation events.[58,96-102] These simulations model the ionic flux, *J*, of species *i* through a nanopore with the flux equation

$$J_i = -D_i \nabla C_i - \frac{z_i F}{RT} D_i C_i \nabla \Phi + C_i v \qquad (1.6)$$

and the Poisson equation modeling the charge density ρ:

$$\nabla^2 \Phi = -\frac{\rho}{\varepsilon \varepsilon_0} \qquad (1.7)$$

where *D*, *C*, *z* are the diffusion coefficient, concentration, and charge of the ionic species *i* in solution, respectively. *F*, *R*, *T,* and ε_0 are respectively Faraday's constant, the gas constant, the temperature, and permittivity of free space. Additionally, Φ is the electric potential, v is solution velocity, and ε is the relative permittivity of the solution. Equation 1.6 and 1.7 can be used to predict the mass transport resistance and the current flowing through the pore.[58,74] Figure 1.3 shows results from finite-element software modeling the localization of the electric field, and thus the sensing zone, at the tip of a glass nanopore membrane where only the profile of the pore is depicted in 2-D axial symmetry. The current-pulse due to a particle translocation can also be modeled as a function of the particle's movement through a pore.[58] This allows for quantitative

a)

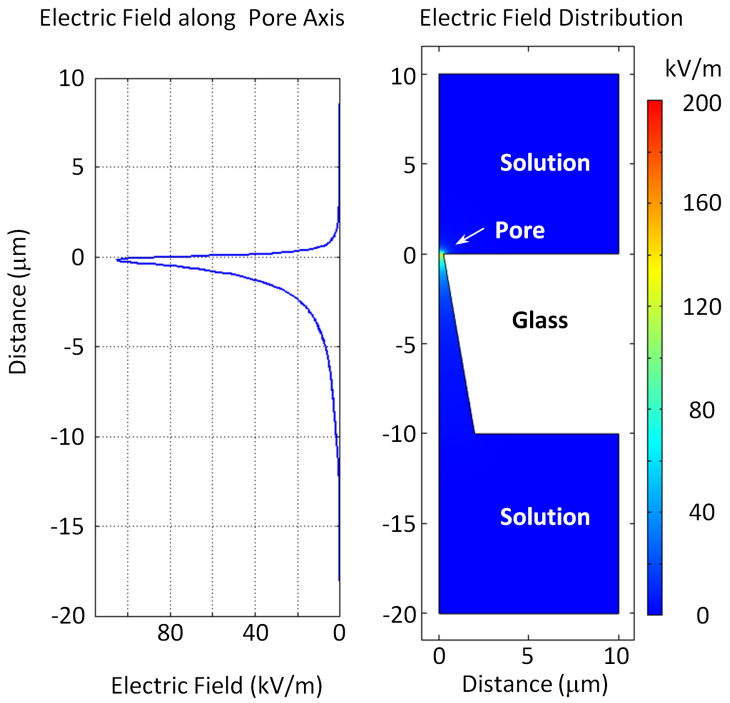

b)

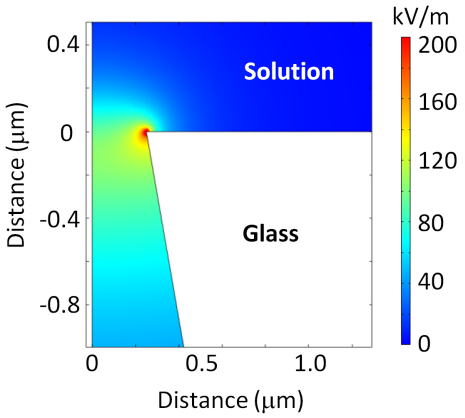

Figure 1.3 a) Results from finite-element simulations depicting the electric field in a 250 nm radius nanopore embedded in an uncharged glass membrane with an applied voltage of 0.2 *V* across the nanopore and a KCl concentration of 25 mM. The line profile represents the electric field through the center axis of the pore. b) An expanded section of the pore orifice.

comparison experimental results and leads to a better understanding of the mechanism involved in the translocation process.

In this dissertation we use the GNM as the platform for the resistive-pulse detection of both liposomes and microgels while applying pressure and/or voltage to drive the particles through its orifice. Additionally, we use finite-element simulations to model the electric field in the sensing zone and compare simulated results to the translocation of nanoparticles though the glass nanopore membrane. Chapters 2 and 3 specifically deal with the translocation of 570 nm radius microgels as they deform and desolvate during translocation under pressure through pores of smaller dimensions. Translocation event rates, durations, and current-pulse heights are investigated and found to be functions of the conductivities of the microgel and the surrounding solution. Chapter 4 investigates the translocation of multilamellar liposomes as they translocate through pores both larger and smaller than the liposomes. Additionally, the rigidness of the liposome's bilayer is explored as a function of the temperature and is reflected in the ability of the liposome to translocate through pores of smaller dimensions than the liposome.

1.5 References

(1) Illum, L; Khan, M. A.; Mak, E.; Davis, S. S. *Int. J. of Pharm.* **1986**, 30, 17-28.

(2) Arinda, M.; Ghandehari, H. *J. of App. Toxicology* **2010**, 30, 212-217.

(3) Kulkarni, P. R.; Yadav, J. D.; Vaidya, K. A., *Int. J. Curr. Pharm. Res*. **2011**, 2, 10-18.

(4) Alsarra, I. A.; Hamed, A. Y.; Alanazi, F. K.; El Maghraby, G. M., *Neuromethods* **2010**, 45, 175-203.

(5) Lasic, D. D.; Papahadjopoulos, D., *Medical Applications of Liposomes*, New York: Elsevier 1998.

(6) Tran, M. A.; Watts, R. J.; Robertson, G. P., *Pigment Cell & Melanoma Res*. **2009**, 22, 388-399.

(7) Maeda, H.; Bharate, G. Y.; Daruwalla, J. *Eur. J. Pharm. Biopharm*. **2009**, 71, 409-419.

(8) Mitragotri, S.; Lahann, J. *Nat. Mater*. **2009**, 8, 15-23.

(9) Nel, A. E.; Madler, L.; Velegol, D.; Xia, T.; Hoek, E. M. V.; Somasundaran, P.; Klaessig, F.; Castranova, V.; Thompson, M. *Nat. Mater*. **2009**, 8, 543-557.

(10) Gelperina, S. *Drugs and the Pharmaceutical Sciences* **2006**, 159, 273-318.

(11) Elder, A.; Vidyasagar, S.; De Louise, L. *Nanomedicine and Nanobiotechnology* **2009**, 1, 434-450.

(12) Nel A.; Xia, T.; Madler, L.; Li, N. *Science* **2006**, 211, 622-627.

(13) Brannon-Peppas, L.; Blanchette, J. O. *Advanced Drug Delivery Reviews* **2004**, 56, 1649-1659.

(14) Buzea, C.; Pacheco, I. I.; Robbie, K. *Biointerphases* **2007**, 2, MR17-MR71.

(15) Langer, R. S. *Science* **1990**, 249, 1527-1533.

(16) Uhrich, K. E.; Cannizzaro, S. M.: Langer, R. S.; Shakesheff, K. M. *Chem. Rev*. **1999**, 99, 3181-3198.

(17) Pillai, O.; Panchagnula, R. Curr. *Opin. Chem. Biol*. **2001**, 5, 447-451.

(18) Champion, J. A.; Katare, Y. K.; Mitragotri, S. *J. Controlled Release*, **2007**, 121, 3-9.

(19) Ruiz-Hernandez, E.; Lopez-Noriega, A.; Acros, D.; Vallet-Regi, M. *Engineering Materials* **2010**, 441, 333-355.

(20) Ramesh, B.; Ganesh, N. S.; Raju, K. N. S. L.; Kavitha, K. *J. Pharm. Res*. **2011**, 4, 1688-1690.

(21) Granqvist, C. G.; Buhrman, R. A. *Phys. Rev. Lett*. **1976**, 37, 625-629.

(22) DeBlois, R. W.; Bean, C. P. *Rev. Sci. Instrum*. **1970**, 41, 909-906.

(23) DeBlois, R. W.; Wesley, R. K. A. *J.Virol*. **1977**, 23, 227-233.

(24) Furlani, E. P. *Materials* **2010**, 3, 2412-2446.

(25) Moretti, M.; Di Fabrizio, E.; Cabrini, S.; Musetti, R.; De Angelis, F.; Firrao, G. *Biosensors and Bioelectronics* **2008**, 24, 141-147.

(26) Beveridge, J. S.; Stephens, J. R.; Williams, M. E. *Annu. Rev. Anal. Chem*. **2011**, 4, 251-273.

(27) Firnkes, M. Pedone, D.; Knezivic, J.; Doblinger, M.; Rant, U. *Nano Lett*. **2010**, 10, 2162.

(28) Fologea, D.; Ledden, B.; McNabb, D. S.; Li, *J. Appl. Phys. Lett*. **2008**, 91, 053901.

(29) Mohammad, M. M.; Prakash, M.; Matouschek, A.; Movileanu, L. *J. Am. Chem. Soc*. **2008**, 130, 4081.

(30) Uram, J. D.; Mayer, M. *Biosensors and Bioelectronics*. **2007**, 22, 1556-1560

(31) Bayley, H.; Martin, C. R. *Chem. Rev*. **2000**, 100, 2575-2594.

(32) Choi, Y.; Baker, L. A.; Hillebrenner, H.; Martin, C. R. *Phys. Chem. Chem. Phys*. **2006**, 8, 4976-4988.

(33) Luo, M.-B. *Polymer* **2007**, 48, 7679-7686.

(34) Uran, J. D.; Ke, K.; Hunt, A. J.; Mayer, M. *Small* **2006**, 2, 967.

(35) Bangs Laboratories, Inc. 9025 Technology Drive Fishers, IN 46038-2886.

(36) Ted Pella, Inc. P.O. Box 492477, Redding, CA 96049-2477.

(37) Storm, G.; Sahoo, S. K.; De, T. K.; Ghosh, P. C.; Maitra, A.; Ghosh, P. K. *Advanced Drug Delivery Reviews* **1995**, 17, 31-48.

(38) New, R. R. C. *Liposomes: A Practical Approach*. Oxford University Press: New York 1990.

(39) Phillippot, J. R.; Schuber, F., *Liposomes as Tools in Basic Research and Industry*. Boca Raton: CRC Press, 1995.

(40) Pelton, R.; Adv. *Colloid Interface Sci*. **2000**, 85, 1-33.

(41) Hoare, T.; Pelton, R., *Langmuir* **2004**, 20, 2123-2133.

(42) Kim, J.; Serpe, M. J.; Lyon, L. A. *Angew. Chem. Int. Ed*. **2005**, 44, 1333-1336.

(43) Suarez, I. J.;Fernandez-Nieves, A.; Marquez, M. *J. Phys. Chem. B*. **2006**, 110, 25729-25733.

(44) Hendrickson, G. R.; Lyon, L. A. *Angew. Chem. Int. Ed*. **2010**, 49, 2193-2197.

(45) Pecora, R. *J. Nanoparticle Res.* **2000**, 2, 123-131.

(46) Chu, B.; Liu, T. *J. Nanoparticle Res*. **2000**, 2, 29-41.

(47) Popp, N.; Kutuzov, S.; Boker, A., *Adv. Polym. Sci.* **2010**, 228, 39-58.

(48) Wang, Z. L. *J. Phys. Chem. B.* **2000**, 104, 1153-1175.

(49) Leppard, G. G. *Current Nanoscience* **2008**, 4, 278-301.

(50) Jose-Yacaman, M.; Avalos-Boria, M. *Catal. Rev. - Sci. Eng*. **1992**, 34, 55-127.

(51) Allen, T.; *Particle Size Measurement*, Chapman and Hall London 1981.

(52) Allen, T.; *Particle Size Measurement; Powder Sampling and Particle Size Measurement*; Springer 1997.

(53) W. H. Coulter. Means for Counting Particles Suspended in a Fluid. US Patent No. 2656508. Oct. 20, 1953.

(54) Murray, R. W. *Chem. Rev*. **2008**, 108, 2688-2720.

(55) Holden. D. A.; Hendrickson, G.; Lyon, L. A.; White, H. S. *J. Phys. Chem. C*. **2011**, 115, 2999–3004.

(56) Giddings, J. C. *Unified Separation Science*; Wiley: New York, 1991.

(57) Davis, J. M.; Giddings, J. C. *Anal. Chem*. **1983**, 55, 418-424.

(58) Lan, W.-J.; Holden, D. A.; Zhang, B.; White, H. S. *Anal. Chem*. **2011**, 83 , 3840–3847.

(59) Henriquez, R. R.; Ito, R.; Sun, L.; Crooks, R. M. *Analyst* **2004**, 129, 478-482.

(60) Lines, R. W. In *Particle Size Analysis*; Stanley-Wood, N. G., Lines, R. W., Eds; Royal Society of Chemistry: Cambridge, U.K. 1992.

(61) Keyser, U. F. *J. R. Soc. Interface* **2011**, 8, 1369-1378.

(62) Lee, S.; Zhang, Y.; Harrell, C. C.; Martin, C. R.; White, H. S. *Anal. Chem*. **2004**, 76, 6108-6115.

(63) Petrossian, L.; Wilk, S. J.; Joshi, P.; Goodnick, S. M.; Thornton, T. J. *J. Phys. Conf. Ser*. **2008**, 109, 012028.

(64) Fologea, D.; Gershow, M.; Ledden, B.; McNabb, D. S.; Golovchenko, J. A.; Li, J. *Nano Lett*. **2005**, 5, 1905.

(65) Giehart, B. C.; Howitt, D. G.; Chen, S. J.; Zhu, Z.; Kotecki, D. E.; Smith, R. L.; Collins, S. D. *Sens. Actuators B* **2008**, 132, 593-600.

(66) Sun, L; Crooks, R. M. *J. Am. Chem. Soc*. **2000**, 122, 12340-12345.

(67) Zhang, B.; Wood, M.; Lee, H. *Anal. Chem*. **2009**, 81, 5541-5548.

(68) Ito, T.; Sun, L.; Crooks, R. M. *Anal. Chem*. **2003**, 75, 2399-2406.

(69) Han, A.; Schurmann, G.; Mondin, G.; Bitterli, R. A.; Hagelbach, N. G.; de Rooij, N. F.; Staufer, U. *Appl. Phys. Lett*. **2006**, 88, 093901.

(70) Harrell, C. C.; Choi, Y.; Horne, L. P.; Baker, L. A.; Siwy, Z. S.; Martin, C. R. *Langmuir* **2006**, 22, 10837-10843.

(71) Sexton, L. T.; Horne, L. P.; Sherrill, S. A.; Bishop, G. W.; Baker, L. A.; Martin, C. R. *J. Am. Chem. Soc*. **2007**, 129, 13144-13152.

(72) Sexton, L. T.; Mukaibo, H.; Katira, P.; Hess, H.; Sherrill, S. A.; Horne, L. P.; Martin, C. R. *J. Am. Chem. Soc*. **2010**, 132, 6755-6763.

(73) Li, N.; Yu, S.; Harrell, C.; Martin, C. R. *Anal. Chem*. **2004**, 76, 2025.

(74) Lan, W. J.; Holden, D. A.; Liu, J.; White, H. S. *J. Phys. Chem. C* **2011**, 115 (38), 18445–18452.

(75) Holden, D. A.; Hendrickson, G. R.; Lan, W. J.; Lyon, L. A.; White, H. S. *Soft Matter* **2011**, 7, 8035-8040.

(76) Zhang, B.; Galusha, J.; Shiozawa, P. G.; Wang, G.; Bergren, A. J.; Jones, R. M.; White, R. J.; Ervin, E. N.; Cauley, C. C.; White, H. S. *Anal. Chem*. **2007**, 79, 4778-4787.

(77) Ho, C.; Qiao, R.; Heng, J. B.; Chatterjee, A.; Timp, R.J.; Aluru N. R.; Timp, G. *Proc. Natl. Acad. Sci. U.S.A*. **2005**, 102, 10445.

(78) Tabard-Cossa, V.; Trivedi, D.; Wiggin M.; Jetha, N. N.; Marziali, A. *Nanotechnology* **2007**, 18, 305505-305511.

(79) Smeets, R. M. M.; Keyser, U. F.; Dekker, N. H.; Dekker, C. *Proc. Natl, Acad. Sci. U.S.A*. **2008**, 105, 417-421.

(80) Dimitrov, V.; Mirsaidov, U.; Wang, D.; Sorsch, T.; Mansfield, W.; Miner, J.; Klemens, F.; Cirelli, R.; Yemenicioglu, S.; Time, G. *Nanotechnology* **2010**, 21, 065502-065513

(81) Uram, J. D.; Ke, K.; Mayer, M. *ACS Nano* **2008**, 2, 857-872.

(82) Willmott, G. R.; Parry, B. E. T. *J. Appl. Phys*. **2011**, 109, 094307.

(83) Willmott, G. R.; Vogel, R.; Yu S. S. C.; Groenwegen, L G.; Roberts, G. S.; Kozak, D.; Anderson, W.; Trau, M. J*. Phys: Cond. Matt*. **2010**, 22, 454116-454127.

(84) Zhang, H.; Chon. C. H.; Pan X.; Li, D. *Microfluid Nanofluid* **2009**, 7, 739-749.

(85) Piruska, A.; Gong, M.; Sweedler, J. V.; Bohn, P. W. *Chem. Soc. Rev*. **2010**, 39, 1060-1072.

(86) Song, Y.; Zhang, H.; Chon, C. H.; Pan, X.; Li, D. *Sensors and Actuators B*. **2011**, 155, 930-936.

(87) Kovarik M. L.; Jacobsen, S. C. *Anal. Chem*. **2008**, 80, 657-664.

(88) Guo, P.; Hall, E. W.; Schirhagl, R.; Mukaibo, H.; Martin, C. R.; Zan, R. W. *Lab Chip*, **2012**, 12, 558-561.

(89) Sheng, Y.; Bowser, M. T. *Analyst*, **2012**, 137, 1144-1151.

(90) Bard, A. J.; Faulkner, L. R., *Electrochemical Methods*, John Wiley and Sons, Inc., 2001**.**

(91) Siwy, Z. S.; Gu, Y.; Sphor, H. A.; Baur, D.; Wolf-Reber, A.; Sphor, R.; Apel, P.: Korchev, Y. E. *Europhys. Lett*. **2002**, 60, 349-355.

(92) Cervera, J.; Schiedt, B.; Ramirez, P. *Europhys. Lett*. **2005**, 71, 35-41.

(93) Woermann, D. *Nucl. Instrum. Methods* B **2002**, 60, 349-355.

(94) Woermann, D. *Phys. Chem. Chem. Phys*. **2003**, 5, 1853-1858.

(95) Woermann, D. *Phys. Chem. Chem. Phys*. **2004**, 6, 3130-3132.

(96) Wei, C.; Bard, A. J.; Feldberg, S. W. *Anal. Chem*. **1997**, 69, 4627-4633.

(97) Siwy, Z. *Adv. Funct. Mater*. **2006**, 16, 735-746.

(98) Siwy, Z.; Heins, E.; Harrell, C. C.; Kohli, P.; Martin, C. R. *J. Am. Chem. Soc*. **2004**, 126, 10850-10851.

(99) Kosinska, I. D. *J. Chem. Phys*. **2006**, 124, 244707-7.

(100) Fulinski, A.; Kosinska, I. D.; Siwy, Z. S. *Europhys. Lett*. **2004**, 67, 683-689.

(101) Cervera, J.; Schiedt, B.; Neumann, R.; Mafe, S.; Ramirez, P. *J. Chem. Phys*. **2006**, 124, 104706.

(102) Zimmerli, U.; Koumoutsakos, P. *Biophys. J.* **2008**, 94, 2546-2557

CHAPTER 2

RESISTIVE-PULSE ANALYSIS OF MICROGEL DEFORMATION DURING NANOPORE TRANSLOCATION

2.1 Introduction

In this chapter we report investigations of the deformation of microgels as they are driven at low applied pressures through a nanopore in a thin glass membrane.[1] Translocation of soft, deformable particles through small orifices is of interest due to the growing realization that the nanoparticle's physical properties play an important role in biological processes such as cellular uptake, organ localization, extravasation into tumors, and excretion.[2,3] Hendrickson and Lyon recently reported pressure-driven translocation of microgels through a polymeric, track-etched membrane containing a high density of cylindrical pores.[4] In those experiments, microgels were driven through nanopores with diameters tenfold smaller than the unperturbed particle diameter, under hydrostatic pressures relevant to renal filtration. Translocation of a large, soft, hydrated particle through a small pore requires significant deformation, and perhaps desolvation of the particle, and is thus anticipated to be a function of the particle's material properties, the size of the particle and pore, and the surface forces between particle and pore (e.g., electrostatic forces). The mechanism by which a soft polymeric particle enters into a nanopore, deforms to the pore geometry, and

passes through the pore interior is virtually unexplored. While the above-mentioned investigations using track-etched membranes demonstrated microgel translocation through small pores, they do not provide direct insight into the mechanism of microgel deformation during translocation. Herein, we demonstrate that resistive-pulse methods can be used to investigate microgel translocation, providing a means to directly measure the dynamics of single particle deformation from electrical current-time (*i*-*t*) traces.

Resistive-pulse techniques have been used for decades to count and measure the size of particles, in addition to measuring particle-pore interactions.[5-9] These methods are based on measuring a decrease in the ionic current that occurs when the particle, driven by pressure or electrophoretic forces, passes through an opening or channel connecting two electrolyte solutions. For solid particles, translocation occurs only when the particle size is smaller than the pore, whereas a method based on particle "capture and release" has been proposed for detection of solid particles that are larger than the opening.[10] In addition, translocation of small molecules and biomolecules through synthetic and biological nanopores has been extensively investigated using the resistive-pulse technique.[11-19] The conformational flexibility of macromolecules, especially biopolymers, facilitates entry into the pore. For example, Fologea et al. demonstrated that ssDNA translocates through a 4 nm radius solid-state nanopore both in folded or unfolded states, producing conformation-dependent signatures in the ionic current. Similarly, the electric-field driven translocation of ssDNA through a protein with a very small pore opening (e.g., α-hemolysin)

requires threading of the end of the DNA molecule into the protein, followed by unfolding of the DNA secondary structure as the molecule passes linearly, base-by-base, through the protein channel.

2.2 Experimental Methods

2.2.1 Chemicals and Solutions

All solutions were prepared in water obtained from a Barnstead E-pure purification system (>18 MΩ·cm). All chemicals, including KCl, K_2HPO_4, and KH_2PO_4 (Mallinckrodt Chemicals), were used without further purification.

2.2.2 570 nm Radius Microgels

Poly(*N*-isopropylacrylamide-*co*-acrylic acid) microgels were originally prepared and sized by a process described elsewhere.[4] Samples were initially freeze-dried and then re-dispersed at 0.001 wt% in buffered KCl solutions.

2.2.3 GNM Fabrication

All experiments were performed by using a glass nanopore membrane (GNM), prepared by a process previously explained, but briefly summarized here.[21] First, a short length of 25 μm Pt wire was electrochemically sharpened by immersing the tip of the Pt wire in a 6 M NaCN solution with 0.1 M NaOH, and etching the Pt by applying a 100 – 300 Hz ac wave at 3.6 – 4.0 V (peak to peak) vs. a large Pt counter electrode until an ultra-sharp tip is achieved. The Pt tip is then inserted into either a borosilicate or soda-lime glass capillary and flame sealed to a depth between 20 and 70 μm. The excess sealed glass is polished away until a Pt disk is exposed. Further polishing is used to remove additional

material creating larger Pt disks and ultimately larger pores. The disk radius, *r*, may be determined by measuring the diffusion limited current, i_{lim}, in a known redox solution (5 mM ferrocene in acetonitrile) with excess electrolyte (0.1 M $TBAPF_6$) and using the ultra-microelectrode steady-state diffusion-limited current relation:

$$i_{lim} = 4nFDCr \qquad (2.1)$$

where *F* is Faraday's constant, and *D*, *C*, and *n* are the diffusion coefficient, the concentration of the redox molecule, and the number of electrons involved in the redox process, respectively.[20,21] The Pt is then electrochemically etched out (at 4 Vac and 4 kHz vs. a Pt counter electrode) of the pore in a 20% calcium chloride solution resulting in a small conical nanopore embedded in the end of a glass capillary. The radius, *r*, of the small orifice of the GNM is then recalculated by measuring the ionic resistance, *R*, in a 1 M KCl solution and using equation 2.2.[21]

$$r = 0.185/R \qquad (2.2)$$

where the constant 0.185 has units of nm·GΩ.

GNMs are further modified to remove excess surface charge by chemically reacting the exposed surface silanol groups on the glass with either 3-cyanopropyldimethylchlorosilane or trimethylchlorosilane after rinsing with copious amounts of water, dilute nitric acid, ethanol, and acetonitrile. The reaction is performed by immersing the pore in a 2% solution of the silane in acetonitrile overnight followed by rinsing with acetonitrile, ethanol, and water.[21]

2.2.4 Experimental Setup

The internal and external solutions of the capillary contained buffered KCl solution. A constant potential of +0.1 V was applied between two Ag/AgCl electrodes, one positioned in the internal solution and the other located in the external solution. The current was measured by a Dagan Cornerstone Series Chem-Clamp voltameter/amperometer, using a high-sensitivity preamplifier (0.05 to 10 nA/V) and filtered using a 10 kHz 3-pole low-pass Bessel filter. The instrument was interfaced to a PC through a BNC 2120 board (National Instruments) and a PCI 6251 DAQ card (National Instruments). Data was recorded at 150 kHz using in-house virtual instrumentation written in LabVIEW 8.6 (National Instruments). A pressure of -50 mmHg was applied across the nanopore (internal vs. external) using a gas tight syringe attached to the capillary.

2.3 Results and Discussion

2.3.1 Experimental Conditions

The deformation of 570 ± 50 nm radius poly(*N*-isopropylacrylamide-*co*-acrylic acid) (pNIPAm-AAc) microgels during translocation was investigated using glass nanopore membranes (GNM). A schematic diagram of the experimental setup used to investigate microgel deformation during translocation is shown in Figure 2.1. The GNM is a ~50 μm thick soda-lime glass membrane containing a single conically-shaped pore; the membrane is located at the end of

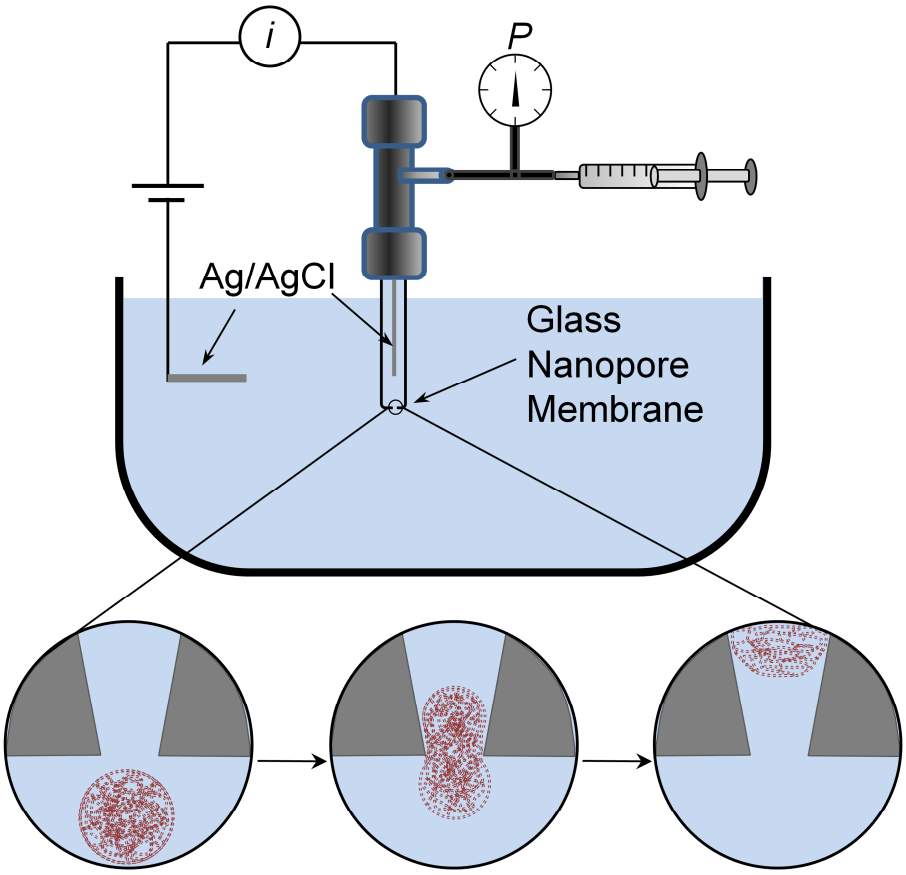

Figure 2.1 Schematic drawing of the experimental setup and microgel deformation during translocation. The glass nanopore membrane (GNM) contains a single nanopore separating two electrolyte solutions. A pressure applied across the GNM drives the external electrolyte solution containing the microgels through the nanopore. A constant voltage is applied between the Ag/AgCl electrodes to record the *i-t* trace.

a glass capillary, separating internal and external electrolyte solutions. The radii of the small orifice of the GNMs used in this investigation were determined by measuring the nanopore conductance in a 1 M KCl solution.[21] A pressure of -50 mmHg was applied across the nanopore (internal vs. external) using a gas tight syringe attached to the capillary, creating a pressure-driven flow of the external electrolyte solution and particles through the nanopore. A constant potential of +0.1 V was applied between two Ag/AgCl electrodes, one positioned in the internal solution and the other located in the external solution. The purpose of the applied voltage is to generate an ionic current through the pore for sensing particle translocation. The applied voltage also generates an electrophoretic force on the negatively charged pNIPAm-AAc microgels, but, as observed experimentally, this force is insufficient to drive the particles through the pore in the absence of an applied pressure, as measured over a range of pressures. The results reported herein are independent of the sign of the applied voltage.

pNIPAm-AAc microgels were synthesized as previously described,[4] and were dispersed at 0.001 wt% in buffered KCl solutions (10 to 130 mM). The average microgel hydrodynamic radius in a 10 mM PBS buffer (100 mM ionic strength, pH 7.4) solution is 570 ± 50 nm, as determined by dynamic light scattering (DLS).[4] The ζ-potential in low ionic strength buffers of pH 7.4 and pH 3.0 was determined to be -20.5 mV and -4.1 mV, respectively, by electrophoretic light scattering. Note that the ζ-potential should not be considered to originate at the microgel surface charge since the “surface” of a microgel is an ill-defined plane. It is almost certainly the case that partially buried charges within the

microgel surface can contribute to the observed mobility. However, ζ-potential values do provide a measure of the relative degree of charging between different microgels or different solution conditions. The microgel acrylic acid concentration was estimated to be ~0.01 M based on AAc synthesis concentration, hydrodynamic radius, and the approximate molecular weight. At pH 7, monomer AAc groups are largely deprotonated (>99.8%, pKa of ~4.25), and are Coulombically balanced by the mobile K^+ from the buffer electrolyte. Thus, the conductivity of the microgel is significant, although the net charge is low.

A microgel passing through the orifice of the pore displaces the electrolyte solution, resulting in a deviation in the pore conductance. The corresponding transient pulse in the *i-t* trace indicates translocation of an individual microgel through this volume. Finite-element simulations demonstrate that the majority of the nanopore resistance (i.e., the sensing zone) is localized to the volume of solution within a few radii of the pore orifice, a consequence of the radially divergent field on both sides of the orifice.[10]

2.3.2 Detection of 570 nm Radius Microgels

Translocation experiments were performed using GNMs with orifice radii ranging between 73 and 910 nm (± 10% error). Figure 2.2 shows *i-t* traces recorded in a buffered 10 mM KCl solution for the translocation of the 570 nm radius microgel particles through a 430 ± 40 nm radius GNM. The shape of the resistive pulse reflects the entry and passage of the particle through the nanopore. Particles driven by convective flow from the bulk external solution encounter the pore orifice on the GNM surface and displace the electrolytic

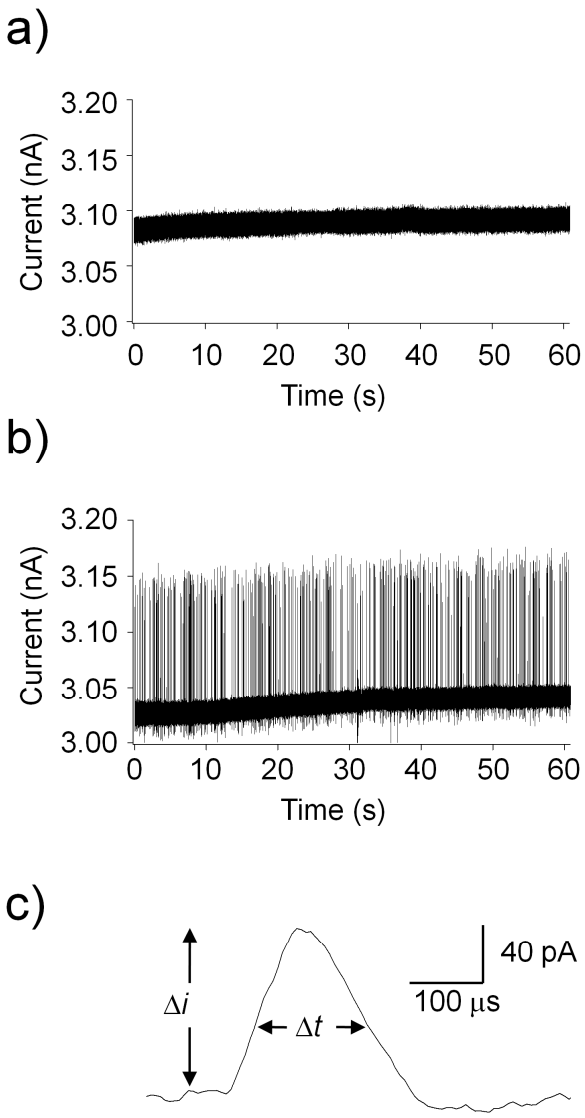

Figure 2.2 Example *i-t* traces of 570 ± 50 nm radius particle translocation events. Traces correspond to data obtained with a 430 ± 40 nm radius pore. A background trace, in the absence of particles, is shown in (a). Particles (0.001 wt%) are driven into the pore using a pressure of -50 mmHg applied across the glass nanopore membrane (internal vs. external). Translocation events over a 60 s period are presented in (b). Expanded image of a single event is shown in (c). The open-pore current (i_o), resistive pulse peak height (Δi), and width at half-peak height (Δt) are indicated on the figure.

solution, causing the current to increase from the baseline value. The observation that the current increases during translocation indicates that the microgel has a higher conductivity that the electrolyte solution, as discussed in more detail below. As the particle deforms under pressure and enters the pore, it begins to fill the interior volume of the pore, resulting in a microgel structure that is pinched down at the orifice (see Figure 2.1). Continued passage of the particle into the expanding nanopore volume allows the particle to relax to its original unconstrained spherical shape. The translocation time (Δt) is defined as the width of the resistive peak at half height, and the resistive-pulse magnitude (Δi) is measured from the baseline i_o, the latter corresponding to the unblocked pore.

In order to verify the resistive-pulses correspond to successful translocations and not to failed entry attempts, we performed experiments in which the pressure, P, across the nanopore was reversed following a period of time in which resistive-pulses were observed. If a resistive-pulse at $-P$ corresponds to a successful translocation, then reversing the direction of electrolyte flow drives the same particle back through the nanopore in the reverse direction at $+P$, producing a corresponding resistive pulse at a later time.

Figure 2.3 shows results of this experiment for a 470 ± 50 nm radius nanopore. Particles were initially placed outside the pore. A positive pressure of +50 mmHg was applied to the interior of the capillary inducing an outward flow of solution and subsequent steady background signal. The pressure was then reversed to -50 mmHg, driving 423 particles through the pore and into in the inner solution. After ~9 s, the pressure was reversed to +50 mmHg and the

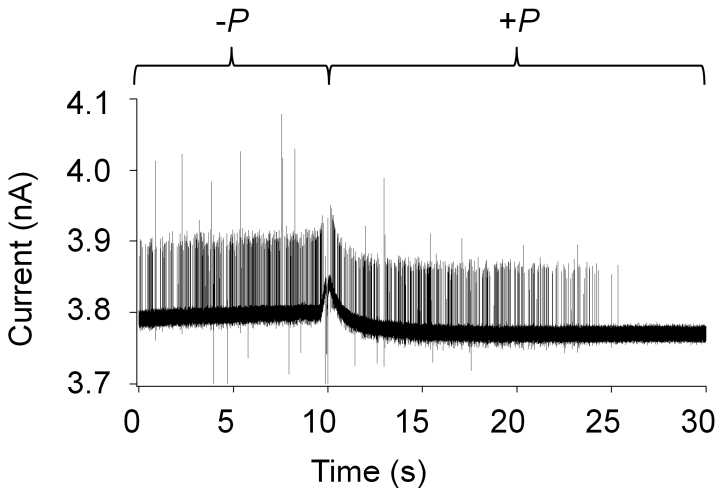

Figure 2.3 Example *i-t* trace of particle translocation at *–P* and reverse translocation at *+P*. Particle translocation through a 470 ± 50 nm radius pore, with an applied voltage of +0.1 *V*. Applied pressure was changed from -50 mmHg to +50 mmHg at time t ≈ 9 s.

captured particles were then pushed back out of the pore, once more passing through the pore orifice and detected a second time. At about 25 s, most of the particles (402) had passed back through the pore and events were no longer observed. The few remaining particles may have adsorbed onto the surface of the glass preventing translocation or diffused far enough into solution that they did not reemerge in the run time of the experiment.

The *i-t* traces for all pores larger than ~375 nm showed forward and reverse translocation for microgel particles with approximately the same number of events recorded before and after pressure reversal. Experiments using GNMs of radii less than ~375 nm resulted in pulses in the *i-t* traces at negative pressure, but the corresponding translocation pulses at positive pressure were not observed. These events correspond to attempted entry of microgels into the nanopore, transiently blocking the pore orifice but resulting in unsuccessful translocation. Additionally, using pores smaller than ~375 nm, microgels were occasionally “captured” for long durations, require reversal of the pressure to dislodge them from the pore mouth (see Figure 2.4) As shown in Figure 2.3, some *i-t* traces contain a small fraction (< 2%) of events corresponding to a decrease in current from the baseline. We speculate that these events correspond to contaminate particles due to their occasional appearance in background traces, as well as in solutions containing the microgels (Figure 2.2).

Previously, Hendrickson and Lyon reported a particle-to-pore ratio as large as 10 for observing translocation of the 570 nm radius microgels through track-etched polycarbonate membranes, corresponding to translocation through

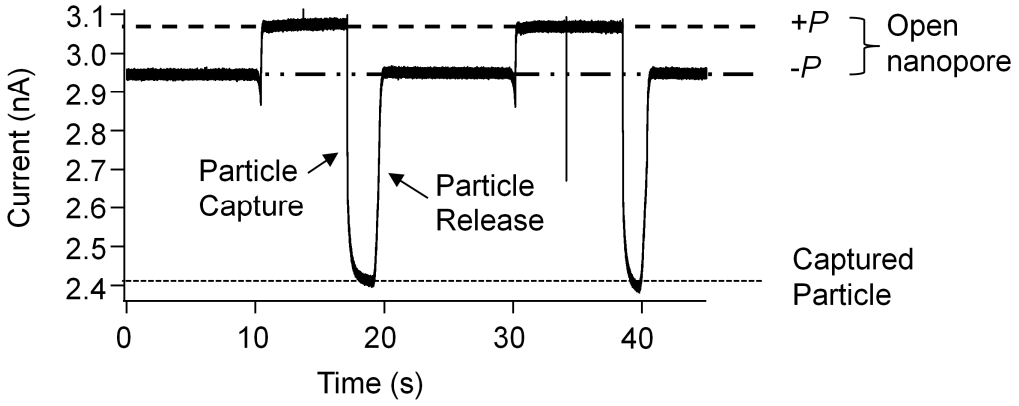

Figure 2.4 An *i-t* trace showing the capture and release of a microgel particle. The experiment was performed using a 360 ± 40 nm GNM in a 10 mM KCl, 1 mM PBS (pH 7) solution, with an applied voltage and pressure of +0.1 *V* and -50 mmHg, respectively (internal vs. external). Particles captured at *–P* are held at the GNM orifice until the pressure is reversed to *+P*. The difference in the currents of the open nanopore at *+P* and *–P* is due to the pressure-dependent ion distribution inside the nanopore.

pores significantly smaller than those employed in the current experiments.[4] We speculate that the negative surface charge at the glass nanopore opening provides a sufficient barrier to passage of the anionic microgels, as opposed to the approximately neutral surface charge of the track-etched polycarbonate membrane pores. Studies of the effects of particle-pore interactions on particle translocation using the resistive-pulse technique are currently underway.

Additionally, resistive-pulses associated with particle translocation through GNMs with radii greater than ~700 nm were not distinguishable from the background current i_o due to the inability to detect the small change in conductivity between the particle and the surrounding solution in a large sensing volume. Additionally, translocation times decrease with increasing pore size due to decreased particle-pore interactions and events may be too fast to be monitored using the current instrumental setup. Reproducible translocation events were observed using GNMs with radii between ~375 and ~600 nm; background *i-t* traces showed no peaks above noise when particles were not present in solution.

A plot of the particle translocation rate as a function of pore size is shown in Figure 2.5 for pores sizes between 70 and 620 nm. As previously discussed, translocation events are not observed for pore sizes below ~375 nm; however a sharp increase in event rate occurs (0 to ~50 s^{-1}) above 375 nm. Above this threshold radius, event rates increase proportionally to the third power of the nanopore radius (r^3), in agreement with the dependence of the volumetric flow rate on the radius as developed by Lan et al. and described by equation 2.3.[22]

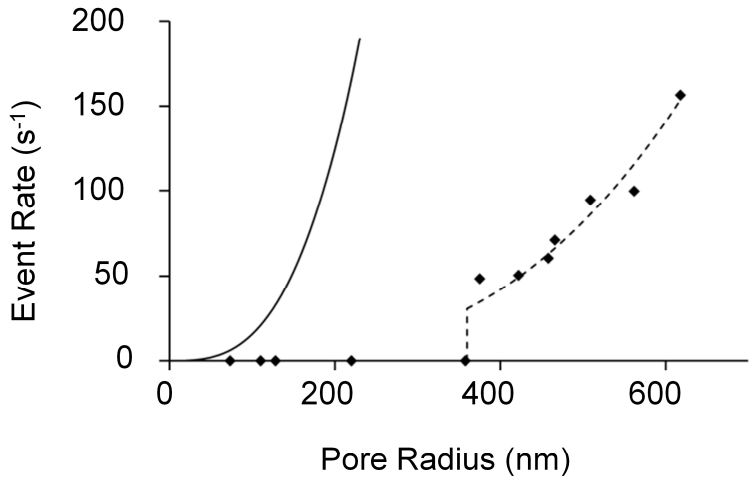

Figure 2.5 Plot of the translocation event rate (events/s) as a function of the nanopore radius. All measurements were made in 0.01 M KCl solutions in a 0.001 wt% particle solution, with an applied voltage and pressure of +0.1 *V* and -50 mmHg, respectively (internal vs. external). Solid line (—) is analytical theory based on pressure driven translocation described by equation 2.3. Dashed line (- - -) is the analytical theory multiplied by best-fitted constant (0.042) above 375 nm and 0 below 375 where translocation was not observed.

$$E.R. = \frac{3\pi r^3 P}{8\eta \cot(\theta)} C \qquad (2.3)$$

where *E.R.* is the event rate, *r* is the radius of the nanopore, *P* is the applied pressure, η is the solution viscosity, θ is the half cone angle of the nanopore, and *C* is the concentration of the nanoparticles.

However, as shown in Figure 2.5, the observed event rate is significantly lower than expected (only 4.2% of theory), although still following the r^3 dependence. This observed low event rate is most likely due to the electrostatic repulsion between the negatively charged GNM and the negatively charged microgel, inhibiting the ability for the microgel to translocate the GNM. As noted above, translocation through pores with radii greater than 700 nm were also observed, but were difficult to discern above the open pore noise. Thus, event rates for these pores cannot be accurately determined.

2.3.3 Determination of Microgel Conductivity

In a 10 mM KCl buffered solution, an increase in the ionic current was observed during 570 nm radius microgel translocation. This increase in current can be understood by considering the ionic conductivity of the microgel relative to the conductivity of the solution volume displaced during translocation. The microgel itself is a porous structure with an estimated AAc concentration of ~0.01 ± 0.01 M. As previously mentioned, at pH 7 nearly all of the acrylic acid groups are dissociated and are charged balanced by mobile K^+. As the particle passes though the pore, the 10 mM electrolyte solution is displaced by the particle, producing an increase in the current due to the higher conductivity of the particle.

A quantitative description of the current increase will require a detailed understanding of not only the nanopore surface charge density, but also the activities and mobilities of the fixed (polymer bound) and mobile ions contained within the microgel.

We further explored the shape of the resistive-pulse on the relative ionic concentrations of the microgel and bulk solution by measuring microgel translocation events using a 430 ± 40 nm pore in electrolyte containing between 10 mM to 130 mM KCl, at pH 7. Resulting translocation times and current deviations are shown in Figure 2.6. Translocation times decreased as ionic concentration increased. The increased ionic concentration causes deswelling of the particles from a radius of 610 ± 60 nm at 10 mM KCl to a radius of 520 ± 50 nm in 130 mM KCl, as determined by DLS. As the particle radius decreases, it requires less interaction and deformation to translocate a pore, resulting in shorter translocation times. In addition, as the bulk solution ionic strength increases, the microgel charges are screened more effectively, thereby lowering the deformation barrier to passage. As noted above, translocation is driven primarily by pressure-induced fluid convection and not by electrophoretic forces; thus, increased electrostatic shielding has little effect on the translocation. A lower limit of Δt ~50 μs for KCl concentrations greater than 60 mM KCl (see Figure 2.6(a)) results from the 10 kHz low-pass filter of the electronic instrumentation.

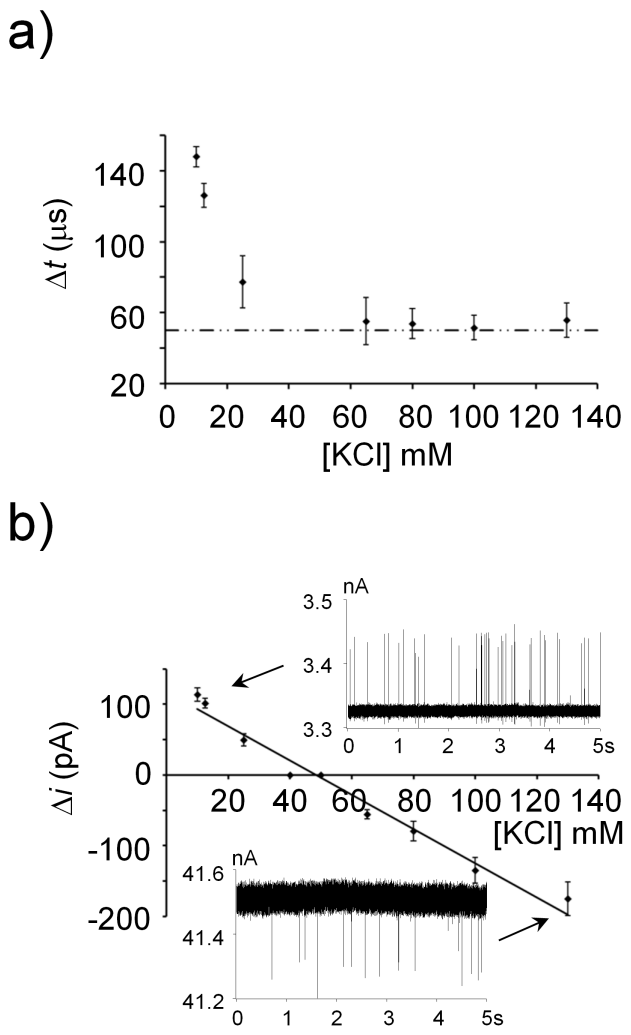

Figure 2.6 Plot of (a) duration time and (b) resistive-pulse height as a function of electrolyte concentration. All measurements were made with 0.001 wt % particles and applied voltage and pressure of +0.1 *V* and –50 mmHg (internal vs. external). Dashed line in (a) represents electronic limitations due to low-pass filter. Insets in (b) show *i-t* traces of particle translocation events.

Pulse-heights as a function of the electrolyte concentration are shown in Figure 2.6(b). The magnitude and sign of the current-pulse is related to the conductance of the particle relative to the electrolyte that the particle displaces during translocation. Figure 2.6(b) shows that at low electrolyte concentrations, particle translocation results in an increase in the current corresponding to a higher particle conductance relative to the surrounding solution. Conversely, at high electrolyte concentration, a decrease in current is observed during translocation corresponding to a relatively lower particle conductance. By fitting a linear relation to the data (slope = -2.4 ± 0.15 pA/mM KCl, intercept = 120 ± 10 pA) and interpolating pulse heights to $\Delta i = 0$, the equivalent conductivity of the particle can be estimated. In this case, the microgels have an ionic conductivity equivalent to a 48 ± 5 mM KCl solution, higher than what is expected if only the 10 mM KCl solution and additional 10 mM K^+, used to charge balance the deprotonated COO^- groups, diffused into the microgel. We speculate that additional conductance is caused by an affinity mobile ions have for the interior structure of the microgel. However, a full understanding will require a detailed knowledge of the chemical properties of the microgel.

2.3.4 Analysis of Event Overlap Probability

In most *i-t* traces, the resistive-pulse magnitudes, Δi, are nearly uniform (< ± 0.2%). However, in some instances (see Figure 2.3) variable peak-heights were observed. In order to determine if these anomalous events are coincident events or correspond to particle aggregates, a Poisson statistical analysis of the probability of overlapping particle translocation events was performed, following

the method described by Davis and Giddings[23,24] for determining the probability of coincident overlap of chromatographic peaks. Poisson statistics yield the expected number of uncorrelated particle translocation events per unit time, λ, and the total observation time, T. The expected number of translocation events, m, in an observation time is given by the equation:

$$m = \lambda T. \tag{2.4}$$

Because the translocation events are of finite duration and occur stochastically, there is a finite probability that two or more events will overlap and be counted as a single event. Thus, the observed number of events may be smaller than the actual number of particles that translocate through the pore.

The probability of single, double, or n-component events is determined as follows. First, the observed events in an observation time T are counted. The time separating the mid-point of two consecutive events is defined as $\Delta\tau$ (See Figure 2.7). The probability that $\Delta\tau$ is greater than the time necessary to resolve these events with baseline resolution, t_o (assumed to be 300 μs), is given by

$$p(\Delta\tau > t_o) = \exp(-\lambda t_o). \tag{2.5}$$

Multiplication of $p(\Delta\tau > t_o)$ by m, followed by substitution of $\lambda = m/T$ (from eq 2.4), yields the number (N) of time intervals between observed events with $\Delta\tau > t_o$ as a function of t_o:

$$N = m\exp(-mt_o/T). \tag{2.6}$$

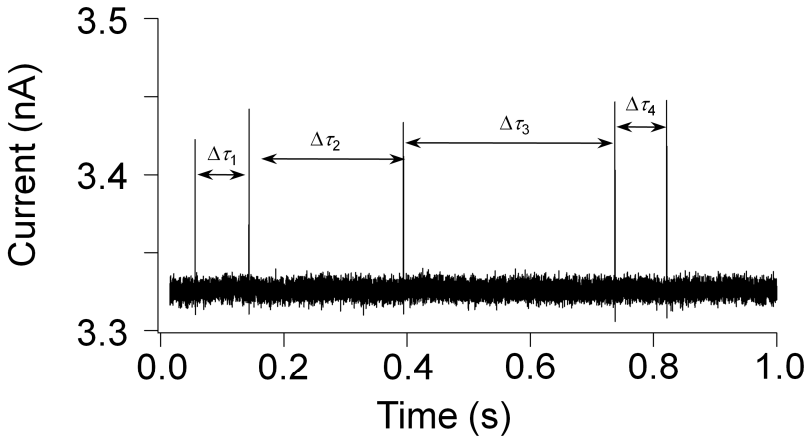

Figure 2.7 A portion of a 60.85 s *i-t* trace recording 570 nm radius microgel particle translocation events through a 430 ± 40 nm radius GNM. The experiment was performed in a 10 mM KCl, 1 mM PBS (pH 7) solution with an applied voltage and pressure of +0.1 *V* and -50 mmHg, respectively (internal vs. external).

Rearranging eq. 2.6 yields:

$$\ln(N) = \ln(m) - m(t_o/T) \quad (2.7)$$

The expected number of observed events, m, is determined by plotting $\ln(N)$ as a function of t_o/T (see Figure 2.8). Both the slope ($-m$) and the intercept ($\ln(m)$) yield m. For the *i-t* data shown in Figure 2.2(b), m was determined to be 427 ± 4 and 431 ± 6, from the slope and intercept, respectively, in excellent agreement with the actual number of observations, 443.

The probability that an individual event represents 1, 2, 3, …, n particle translocation events is given by:

$$N_n = \exp(-2mt_o/T)[1-\exp(-mt_o/T)]^{(n-1)} \quad (2.7)$$

Analysis of the data set presented in Figure 2.2(b) yields a 99.6% probability of any resistive-pulse being a single event where resolution is defined with a peak separation >300 μs. Similarly, the probability of coincident events is negligibly small (the probabilities for double and triple events are 2.1×10^{-3} and 4.4×10^{-6}, respectively), in agreement with the general observation of peaks of uniform magnitude. Thus, an event with an anomalously large peak height likely corresponds to a particle aggregate. Specifically, this was observed when using new samples in which the microgel had not been sufficiently re-dispersed, or older samples in which particles had aggregated.

Finally, Figure 2.9 shows a cluster plot of $\Delta i/i_o$ vs. Δt (bottom left) for the translocation of the 570 ± 50 nm microgels using GNMs of 380 ± 40, 500 ± 50,

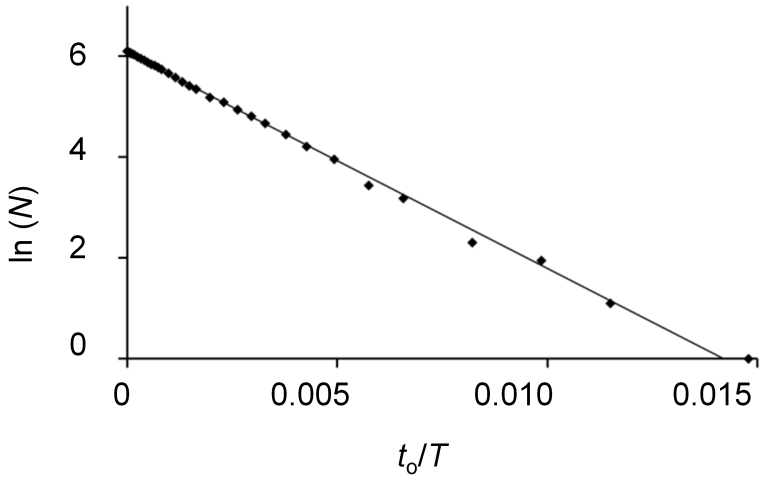

Figure 2.8 Plot of ln(*N*) vs. t_0/T from data described in Figure 2.2(b). Total observation time, *T*, was 60.85 s yielding 443 particle translocation events. The line is a linear regression fit to the data.

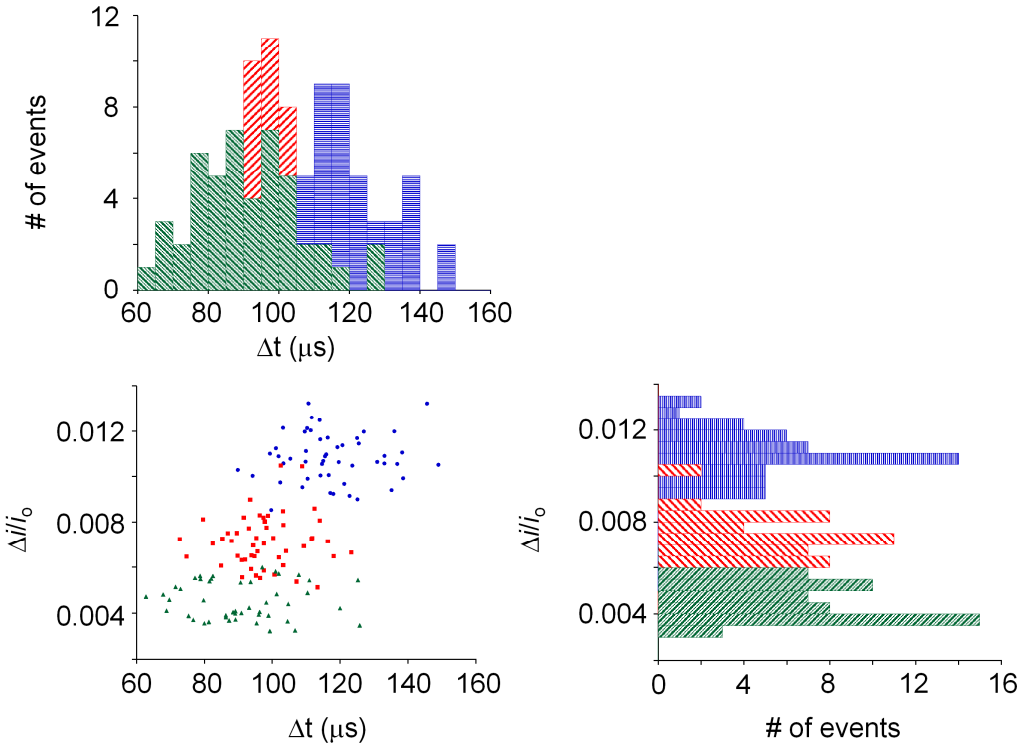

Figure 2.9 Distribution of relative pulse heights ($\Delta i/i_o$) vs. duration times (Δt) of individual translocation events through 380 ± 40 (○), 500 ± 50 (□), and 620 ± 60 (Δ) nm radius pores (N = 50 events for each measurement). A cluster plot of $\Delta i/i_o$ vs. Δt for individual events is shown in lower left. Histograms of Δt and $\Delta i/i_o$ for the same data set are shown at the top and to the right side, respectively.

and 620 ± 60 nm radius. Histograms showing the distribution of Δt and $\Delta i/i_o$ for the same data sets are shown on the top left and bottom right, respectively. The histograms and cluster plot show reasonably sharp distributions of $\Delta i/i_o$ and Δt, reflecting the uniformity of microgel translocation events. The ~15% distribution in $\Delta i/i_o$ observed in Figure 2.9 primarily reflects the true size distribution of the microgel particles determined by DLS (about 10%),[4] in addition to possible spread caused by the mechanical deformation of the microgel as it passes through the pore. An increase in both the average Δt and $\Delta i/i_o$ was observed as the pore size decreases (r^2 = 0.99 for averages and r^2 = 0.38 for individual events). For pore sizes 620, 500, and 380 nm, Δt = 89 ± 17, 98 ± 11, and 117 ± 13 μs and $\Delta i/i_o$ = 0.0045 ± 0.0008, 0.007 ± 0.001, and 0.011 ± 0.001, respectively. The decrease in pore size requires an increase in microgel deformation and interaction with the pore, while also increasing the microgel's occupation of the pore's sensing zone, resulting in both longer Δt and larger $\Delta i/i_o$. The results demonstrated that the resistive-pulse method is able to distinguish different particle-pore interactions.

2.4 Conclusions

We have demonstrated the use of the resistive-pulse method to investigate the kinetics and deformation dynamics of microgel translocation through nanopores. The capability enables a better understanding of the mechanisms and figures of merit for microgel passage through small orifices. Importantly, this approach provides the opportunity to follow individual events in real time, thereby resulting in data that can be directly correlated with the

polymer physics and chemistry of individual microgels. Additionally, the relevance of such deformation events in the development of new drug delivery vehicles is critical; this experimental framework will provide tremendous insight into the design criteria for particles that are able to translocate across biological pores and through tight junctions.

2.5 References

(1) Holden, D. A.; Hendrickson, G.; Lyon, L. A.; White, H. S. *J. Phys. Chem. C*, **2011**, 115(7), 2999-3004.

(2) Mitragotri, S.; Lahann, J. *Nat. Mater*. **2009**, 8(1), 15-23.

(3) Nel, A. E.; Madler, L.; Velegol, D.; Xia, T.; Hoek, E. M. V.; Somasundaran, P.; Klaessig, F.; Castranova, V.; Thompson, M. *Nat. Mater*. **2009**, 8(7), 543-557.

(4) Hendrickson, G. R.; Lyon, L. A. *Angew. Chem. Int. Ed*., **2010**, 49, 2193-2197.

(5) Ito, T.; Sun, L.; Bevan, M.; Crooks, R. M. *Langmuir*, **2004**, 20, 6940-6945.

(6) Petrossian, L.; Wilk, S. J.; Joshi, P.; Goodnick, S. M.; Thornton, T. J. *J. Phys. Conf. Ser*., **2008**, 109, 012028.

(7) Piruska, A.; Gong, M.; Sweedler, J. V.; Bohn, P. W. *Chem. Soc. Rev*., **2010**, 39, 1060-1072.

(8) Giehart, B. C.; Howitt, D. G.; Chen, S. J.; Zhu, Z.; Kotecki, D. E.; Smith, R. L.; Collins, S. D. *Sens. Actuators B*, **2008**, 132, 593-600.

(9) Henriquez, R. R.; Ito, R.; Sun, L.; Crooks, R. M. *Analyst*, **2004**, 129, 478-482.

(10) Lee, S.; Zhang, Y.; Harrell, C. C.; Martin, C. R.; White, H. S. *Anal. Chem*., **2004**, 76, 6108-6115.

(11) Fologea, D.; Gershow, M.; Ledden, B.; McNabb, D. S.; Golovchenko, J. A.; Li, J. *Nano Lett*., **2005**, 5, 1905.

(12) Han, A.; Schurmann, G.; Mondin, G.; Bitterli, R. A.; Hagelbach, N. G.; de Rooij, N. F.; Staufer, U. *Appl. Phys. Lett*., **2006**, 88, 093901.

(13) Bayley, H.; Martin, C. R. *Chem. Re*v. **2000**, 100, 2575-2594.

(14) Choi, Y.; Baker, L. A.; Hillebrenner, H.; Martin, C. R. *Phys. Chem. Chem. Phys.* **2006**, 8, 4976-4988.

(15) Harrell, C. C.; Choi, Y.; Horne, L. P.; Baker, L. A.; Siwy, Z. S.; Martin, C. R. *Langmuir*, **2006**, 22, 10837-10843.

(16) Sexton, L. T.; Horne, L. P.; Sherrill, S. A.; Bishop, G. W.; Baker, L. A.; Martin, C. R. *J. Am. Chem. Soc*., **2007**, 129, 13144-13152.

(17) Sexton, L. T.; Mukaibo, H.; Katira, P.; Hess, H.; Sherrill, S. A.; Horne, L. P.; Martin, C. R. *J. Am. Chem. Soc*., **2010**, 132, 6755-6763.

(18). Deamer, D. W.; Branton, D. *Acc. Chem. Res*. **2002**, 35, 817-825.

(19) Baley, H. *Curr. Opin. Chem. Biol*. **2006**, 10, 628-637.

(20) Bard, A. J.; Faulkner, L. R., *Electrochemical Methods*, John Wiley and Sons, Inc., 2001.

(21) Zhang, B.; Galusha, J.; Shiozawa, P. G.; Wang, G.; Bergren, A. J.; Jones, R. M.; White, R. J.; Ervin, E. N.; Cauley, C. C.; White, H. S. *Anal. Chem*., **2007**, 79, 4778-4787.

(22) Lan, W.-J.; Holden, D. A.; Liu, J.; White, H. S.; *J. Phys. Chem. C*, **2011**, 115 (38), pp 18445–18452.

(23) (a) Davis, J. M.; Giddings, J. C. *Anal. Chem*., **1983**, 55, 418-424.

(24) Giddings, J. C. *Unified Separation Science*; Wiley: New York, 1991.

CHAPTER 3

ELECTRICAL SIGNATURE OF THE DEFORMATION AND DEHYDRATION OF MICROGELS DURING TRANSLOCATION THROUGH NANOPORES

3.1 Introduction

In this chapter we present further investigations into the translocation of the 570 ± 50 nm microgels, specifically dealing with both chemical and physical properties relevent to translocation through porous membranes.[1] Interactions of nanoparticles with biological systems has become of great interest, including research using metal and semiconductor nanoparticles, micelles, liposomes, and hydrogel particles (microgels). The potential application of nanoparticles in the context of biological processes, including excretion, extravasation, cellular uptake, and organ localization,[1-5] for medical therapies and diagnoses requires a detailed understanding of the relationship between nanoparticle properties (e.g., surface charge, porosity, hydrophobicity, and conductivity) and their intended function.[6,7] For example, a recent study by Arinda and Ghandehari showed the influence of size, shape, and various surface properties of gold nanoparticles on cellular uptake into human prostate cancer cells, in an effort to develop a human tumor therapy.[5]

An understanding of translocation of nanoparticles through porous biological media, such as that which occurs in tumor penetration or renal filtration, is critical to the development nanoparticles applications in medicine. In a recent report, Hendrickson and Lyon described the translocation of soft, hydrated particles through a membrane containing nanopores with diameters that were tenfold smaller than the unperturbed particle diameter, at pressure differentials relevant to normal renal filtration conditions.[8] Those experiments demonstrated the deformability of microgels during translocating through a nanoporous membrane. To obtain detailed information on single-particle translocation events, we have applied the resistive-pulse sensing technique to measure the electrical signature associated with the deformation and dehydration of individual microgel particles during translocation through a single nanopore.[9]

The resistive-pulse technique measures changes in the ionic current that occur as an object, driven by convective or electrophoretic forces, translocates a pore connecting two electrolytic solutions.[10] This technique has been applied for detection and analysis of a variety of particles over the past few decades including “solid” spheres, such as gold or polystyrene particles,[11-18] as well as “soft” or flexible particles, often bio-molecules.[19-25] For solid particles, translocation only occurs when the particle is smaller than the pore opening, with particles being “captured” at the orifice when the particle size exceeds the pore size. Pressure or voltage reversal releases the particle and allows for the capture of additional particles.[18] Conversely, for soft particles, such as microgels or biopolymers, translocation through the pore is often facilitated by the

conformational flexibility of the object. For example, Ying et al. recently detected conformational changes in an ATP binding DNA aptamer by monitoring the translocation of the bound and unbound states through an α-hemolysin nanopore.[25] Additionally, we recently reported the first investigations of microgel deformation and translocation through a conical nanopore of dimensions smaller than the microgel, embedded in a thin glass membrane.[9] In those experiments pressure was used to drive the soft, hydrated microgel through the pore. The conductivity of the microgel was determined by monitoring the sign and magnitude of translocation resistive pulses as a function of the bulk electrolyte concentration. Here, we demonstrate that current-time traces of single particle translocation events, obtained with ~100 μs temporal resolution, can be used to measure dynamic changes in the conductivity of the microgel as it compresses and partially dehydrates during translocation.

3.2 Methods and Materials

3.2.1 Solutions

K_2HPO_4, KH_2PO_4, and KCl were obtained from Mallinckrodt Chemicals and were used without further purification. All solutions were prepared using water obtained from a Barnstead E-Pure water purification system (>18 MΩ•cm). Solutions contained 10 mM KCl, buffered at pH 7.0 with 1.0 mM K_2HPO_4 / KH_2PO_4.

3.2.2 Microgels

Poly(*N*-isopropylacrylamide-*co*-acrylic acid) (pNIPAm-AAc) microgels were prepared by precipitation polymerization, as described elsewhere.[8] The synthesis of these microgel yields monodisperse particle sizes and a uniform distribution of AAc throughout the particle.[26,27] Microgels contained 1 mol% *N*,*N*'-methylenebisacrylamide (BIS) and 10 mol% acrylic acid (AAc). The pH-dependent size and zeta potential of these microgels have been previously reported.[8] The microgel hydrodynamic radius at neutral pH was determined by dynamic light scattering (DLS) to be 570 ± 50 nm. Samples were freeze-dried for storage, and later re-dissipated at 0.00025 wt% in phosphate buffered KCl solutions for the translocation experiments.

3.2.3 Translocation Experiments

Translocation experiments were performed using unmodified glass nanopore membranes (GNMs), consisting of a single conical pore embedded in a 25 – 50 μm-thick glass membrane at the end of a glass capillary.[28] The orifice radii of the nanopores used in these experiments ranged from 200 to 700 nm ± 10%. The internal and external solutions were filled with buffered KCl solution, and the Ag/AgCl electrodes were placed on opposing sides of the membrane. A bias of 100 mV was applied to generate a current ranging between 1 and 10 nA. A pressure was applied across the nanopore using a gas tight syringe and monitored with a Traceable Pressure Meter (Fisher Scientific). The current was monitored by using a Dagan Cornerstone Series Chem-Clamp voltmeter/amperometer, with a high sensitivity pre-amplifier (0.05 to 10 nA/V) and

a 10 kHz low-pass Bessel filter. The instrument was interfaced to a PC with a BNC 2021 Board (National Instruments) and a PCI 6251 DAQ card (National Instruments). Data was recorded at 150 kHz, using in-house virtual instrumentation written in LabVIEW 8.6 (National Instruments).

Finite-element simulations were performed on a PC using Comsol Multiphysics 3.5a (Comsol).

3.3 Results and Discussion

3.3.1 Pressure Driven Translocation of pNIPAm-AAC Microgels

Translocation of pNIPAm-AAc microgels through the orifice of a GNM was investigated by monitoring the current-time (*i*-*t*) response. A schematic diagram of the setup is shown in Figure 3.1, where the GNM is a single conical pore embedded in a glass membrane located at the end of a glass capillary. Both internal and external solutions contained 10 mM KCl, buffered with 1.0 mM phosphate at pH 7.0. The current is generated by applying a potential of +100 mV (internal vs. external) between the two Ag/AgCl electrodes. Due to the conical shape of the pore, the majority of the potential drop occurs in the electrolyte volume near the opening of the pore, defined as the sensing zone, vide infra.[18] Microgels were placed in the external solution and driven through the pore by applying a pressure across the membrane with a gas-tight syringe. Microgel translocation was monitored by measuring the change in current when the microgels passed through the sensing zone.

As previously reported, the GNM requires an external pressure to achieve microgel translocation through pores with dimensions smaller than the

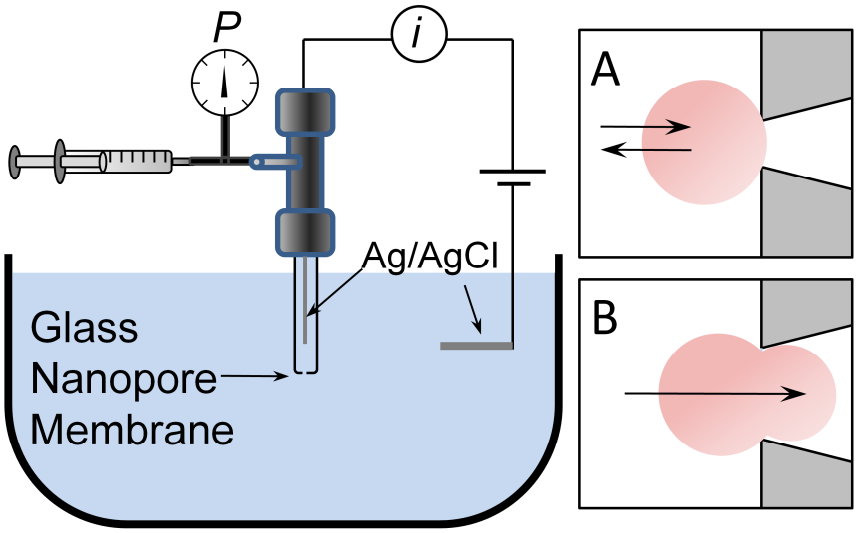

Figure 3.1 Schematic drawing showing the experimental setup. A conical nanopore embedded in a glass membrane separates two buffered solutions containing 10 mM KCl. A voltage (between the Ag/AgCl electrodes) and pressure are applied and the resulting ionic current through the pore is recorded. Particles either (A) block the pore or (B) deform and translocate depending on the nanopore radius and the applied pressure.

microgels.[9] Figure 3.2 shows typical *i-t* traces for a 300 ± 30 nm nanopore submerged in a buffered solution containing (a) no particles but at an applied pressure of -50 mmHg (internal vs. external), (b) 0.00025 wt% microgel at -50 and (c) -150 mmHg. As shown in Figure 3.2a, resistive-pulse events are not observed in the absence of the microgels. For experiments containing microgels, however, transients in the *i-t* traces reflect interactions between the microgels and the pore.

At low pressures (-50 mmHg, Figure 3.2b), the pressure is insufficient to force a 570 ± 50 nm radius microgel though the 300 ± 30 nm radius pore orifice. Thus, blockage is observed where the microgel is trapped at the pore orifice in mid-translocation. These blockages are reversed by applying an opposing pressure, which reverses the direction of solution flow, and forces the trapped microgel away from the pore. In Figure 3.2b, the open-pore current following a particle capture is slightly larger the value preceding capture. This is due to a combination of the influence of solution flow on the mobile charge distribution within the nanopore and a small error in measuring the applied pressure (~5%). An analysis of this phenomenon will be presented elsewhere.

At -150 mmHg (Figure 3.2c), the force is sufficiently large to push the microgel into and through the pore, resulting in a series of resistive pulses, where each pulse corresponds to a single particle translocation event. For a 0.00025 wt% microgel solution and 300 ± 30 nm nanopore, ~12 translocation events occur per second at an applied voltage of 100 mV. During each event, the solution within the pore is replaced by the volume of the microgel, resulting in

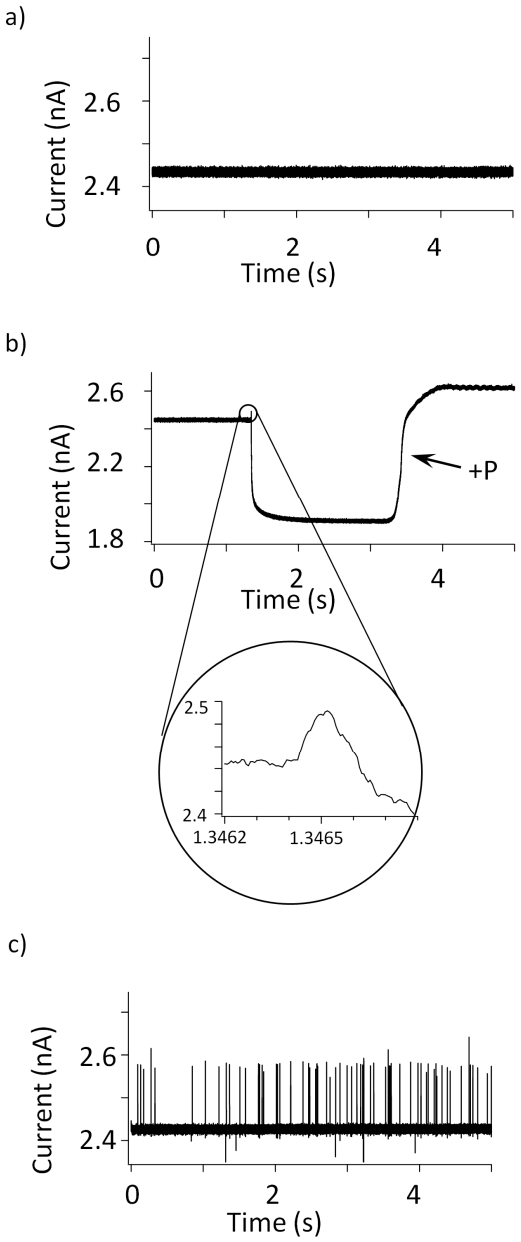

Figure 3.2 *i-t* traces corresponding to experiments with 570 ± 50 nm radius microgels in a 10 mM KCl, 1 mM PBS solution at pH 7.0, using a 300 ± 30 nm radius pore. The applied voltage was +100 m*V* (internal vs. external solution). (a) Background trace at -50 mmHg (internal vs. external) in the absence of particles. (b) and (c) *i-t* traces with 0.00025 wt% microgels at pressures of -50 mmHg and -150 mmHg (internal vs. external solution), respectively.

deviations from the open pore current. The magnitude and sign of the current pulses reflect any difference in conductivity between the microgel and the pore. The pulses recorded in the *i-t* trace of Figure 3.2c correspond to an increase in current during microgel translocation, reflecting the higher conductivity of the particle relative to the 10 mM KCl solution that is displaced within the pore during translocation.[9] As shown below, the *i-t* traces provide fundamental information regarding the chemical and physical states of the microgel during translocation.

Translocation events were differentiated from other types of transient particle-pore orifice interactions by a method previously established.[9,29] Briefly, microgels are initially placed in the external solution, pulled individually into the pore, and captured in the internal solution. The pressure was then reversed and the microgels are driven back out of the pore into the external solution, once again passing through the pore orifice, and detected a second time (data not shown). The number of events observed by flow in one direction corresponds to the number of events observed upon reversal of the flow.

3.3.2 Peak Shape Dependence on Pore Size and Pressure

Figure 3.3 shows expanded *i-t* traces for peaks resulting from individual microgel translocation events. Traces (i) through (v) show the current responses for microgels as they translocate through a 300 ± 30 nm radius pore at pressures ranging between -70 and -150 mmHg. At applied pressures less than 100 mmHg, the translocation response displays two maxima above the open pore baseline current. As the magnitude of the applied pressure is increased, the two peaks merge into a single peak. As seen in Figure 3.3(vi-viii), the same trend is

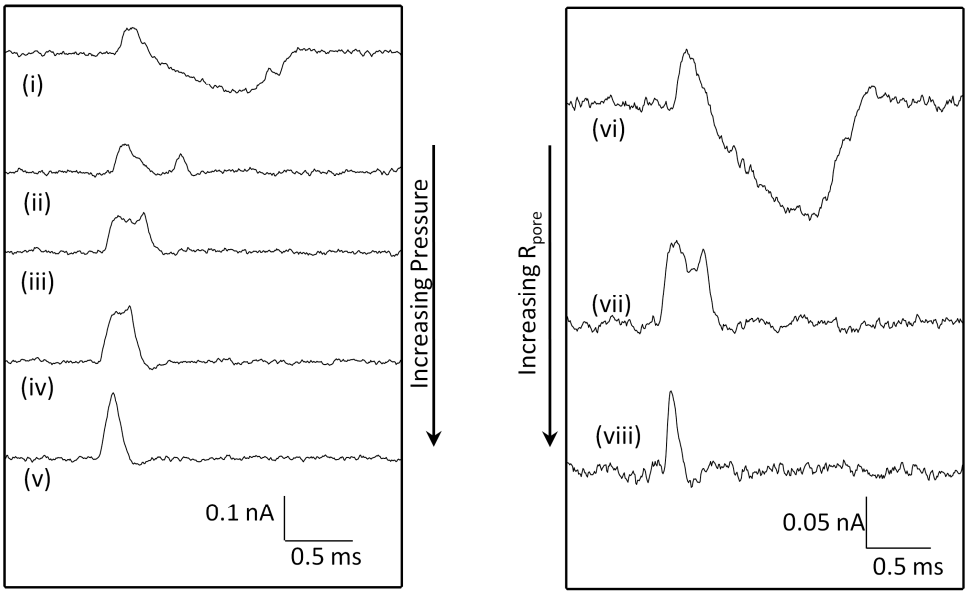

Figure 3.3 Expanded *i-t* traces corresponding to translocation of individual microgels through a GNM. Microgels were dispersed in a 10 mM KCl, 1 mM PBS solution at pH 7. Traces i-v represent events through a 300 ± 30 nm radius pore at applied pressures of (i) -70, (ii) -80, (iii) -100, (iv) -120, and (v) -150 mmHg. Traces v-viii represent events at an applied pressure of -100 mmHg through pores with radius of (vi) 270 ± 30, (vii) 300 ± 30, and (viii) 400 ± 40 nm.

observed as the pressure is held constant at -100 mmHg, and the pore radius is increased from 270 ± 30 to 400 ± 40nm. Translocation times decrease from ~2 ms for the smallest pores and largest pressures, to ~0.2 ms for the largest pores and smallest pressures.

The complex dependence of the peak shape on pressure and nanopore dimensions reflects the deformation of the microgel by the pressure acting on it during translocation. For translocation events where the pore is larger than the microgel, no deformation is required and the microgel simply replaces a portion of the solution in the sensing zone. Because the microgel has a higher conductivity than the 10 mM KCl solution that it displaces, these events increase the overall conductance of the pore, resulting in positive pulses that reflect an increase in current.[9] This is similar to translocation of “hard” non-conducting spherical particles, such as polystyrene, except that the lower conductivity of polystyrene particles results in a decrease in current during translocation.

When the nanopore radius is smaller than that of the microgel, the microgel is forced to deform to the shape of the orifice and pore walls. As the microgel approaches the pore, the higher conductivity of the microgel relative to the solution results in an initial increase in the current, as observed in all *i-t* traces, regardless of the nanopore size relative to that of the microgel. As the microgel squeezes through a pore orifice of smaller dimensions, the compression results in microgel deformation and desolvation. A portion of the microgel solution that contains the mobile K^+ that balance the AAc residues is forced out upon compression, resulting in a decrease in the particle conductivity and thus a

decrease in the observed current. The amount the particle decreases in conductivity is only reaches about 1-3% as observed by experimentation. As the microgel passes through the tightest portion of the pore and into the expanding volume of the pore where the pressure differential is lower, it reabsorbs water and ions. This re-swelling increases its conductivity and the observed current, resulting in a second maximum in the *i-t* trace. We note that the observed translocation times (<2 ms) are of the same order of those predicted based on studies of gel deswelling kinetics.[30,31]

3.3.3 Finite-Element Simulation of Pore-Microgel Interaction

Further insight into the shape of the transient *i-t* trace is gained by examining the electric field distribution within the nanopore. Finite-element simulations were performed to compute the potential distribution across the GNM, as described elsewhere.[12] A 2-dimentional cross-section of the field for a 300 nm radius nanopore is presented in Figure 3.4, as well as a line plot of the field along the center axis of the nanopore. As shown, the electric field extends outside the pore orifice to a distance equal to about 3x the pore orifice radius. The field decays more slowly with distance within the pore interior. A maximum field value of ~20 kV/m occurs near the pore orifice. A microgel moving from the exterior solution into the interior solution experiences a changing electric field during translocation. At position A in Fig 3.4, the microgel is outside the sensing zone and its presence does not affect the ion flux through the pore. However as the microgel approaches the pore opening (Fig. 3.4, position B), a significant overlap with the electric field occurs prior to entering the pore. At this position, no

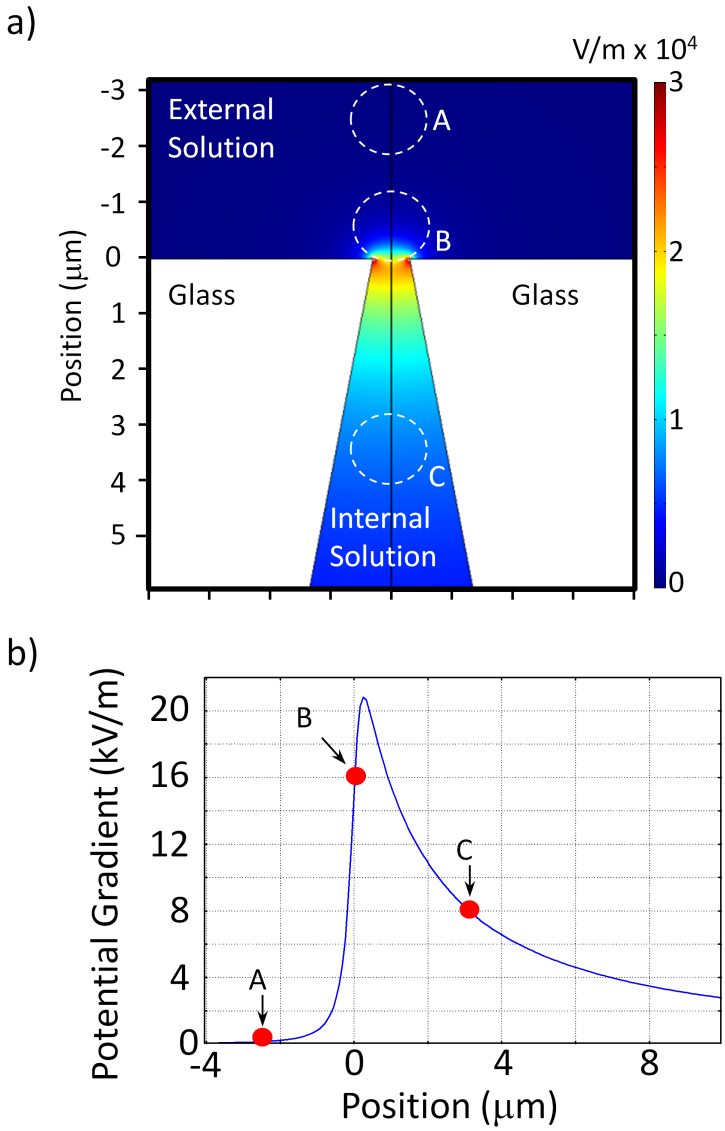

Figure 3.4 Finite-element simulation showing the electric field distribution near the opening of a 300 nm radius nanopore. The simulation was run using conditions reflecting experimental setup: V = +100 m*V*, [KCl] = 10 mM. Bottom trace shows values of electric field through the center axis of the pore. A, B, and C depict positions of the microgel during translocation.

deformation of the microgel is required, but since the microgel has a higher conductivity than the solution it displaces, an increase in current is observed. As the microgel continues into the nanopore, it must deform under the pressure in order to translocate. As this occurs, dehydration results in a decrease in the microgel conductivity causing a minimum in the observed current. Typical dehydration results in the depletion of approximately 1-5% of the ionic conductivity within the microgel. When the microgel proceeds further into the expanding volume of the nanopore, it re-absorbs solution (Fig 3.4, position C) increasing its conductivity, causing a second maximum in the *i-t* trace. Finally, as the microgel travels deep into the pore, it passes out of the sensing zone that is defined by the electric field, and the nanopore current returns to the baseline value.

3.3.4 Microgel Deformability and Compressibility

For translocation events through pores only slightly smaller than the microgel (~450 – 550 nm radius, e.g., trace (viii) of Fig. 3.3), the microgels require minimal deswelling and therefore a smaller depletion of their interior solution and mobile ions. Thus, during translocation, an increase in current is observed as the microgel approaches and passes the nanopore orifice. For small pores (~250 – 350 nm radius), deswelling must be significant in order for passage to occur. At higher pressure, the translocation rate is apparently faster than the effective deswelling rate of the microgels. The single peak suggests that the particle passes through the pore without a large change in volume. However, at lower pressures, the translocation time is longer, with the timescale now being

more commensurate with solvent egress. Thus, the microgel volume decreases enough to observe a change in microgel conductivity during translocation.

Translocation events were not observed for the smallest pores employed (~200 nm) at pressures up to -500 mmHg. Instead, blockage events were observed such as that shown in Figure 3.2b. The *i-t* trace of a blockage event is characterized by an initial increase in current (see inset of Fig. 3.2b), followed by a decrease in current that can be reversed by reversal of the pressure. The initial increase in current is corresponds to the initial approach of the microgel to the pore entrance (position B in Fig. 3.4a) resulting in an increased conductivity within the sensing zone. As the particle begins to enter the pore, it deswells by expelling internal electrolyte solution. For the smallest pores and/or at low pressures, the pressure pushing the microgel through the nanopore is eventually balanced by the increasing internal osmotic pressure within the microgel, preventing further compression and translocation. A blockage occurs if this balance of the inward compressive force and outward osmotic pressure occurs prior to passage through the orifice.

Microgel translocation event rates (number of events/s) vs. applied pressure for various pore-to-microgel size ratios ($R_{pore}/R_{\mu gel}$) were recorded and are presented in Figure 3.5. Event rates display a linear response versus pressure for all $R_{pore}/R_{\mu gel}$. However, a threshold pressure (P_{min}) exists which must be overcome in order to achieve translocation. For pressures less than P_{min}, *i-t* traces show reversible blockage events as depicted in Figure 3.2b.

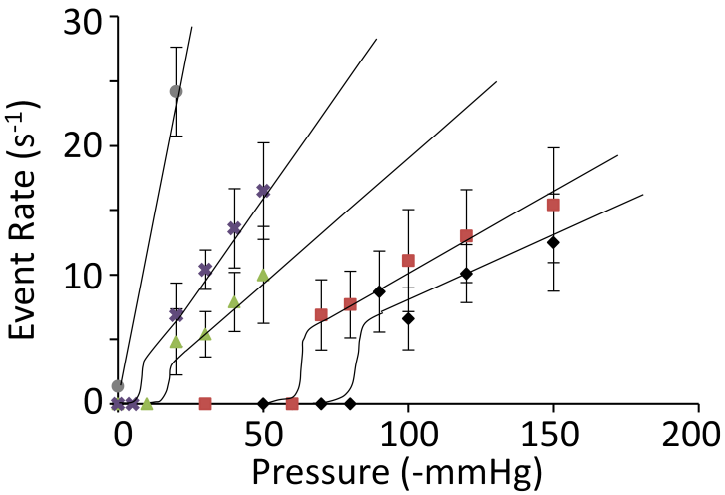

Figure 3.5 Event rates for various $R_{pore}/R_{\mu gel}$ (●, 1.2), (x, 0.8), (▲, 0.6), (■, 0.53), and (♦, 0.47) vs. the applied pressure (internal vs. external). All experiments were carried out using 570 nm radius microgels in a 10 mM KCl, 1 mM PBS solution at pH 7, and an applied voltage of +100 m*V*. Solid lines are drawn as a guide to the eye.

P_{min} is plotted as a function of the $R_{pore}/R_{\mu gel}$ in Figure 3.6, along with the slopes of the event rate vs. pressure plots shown in Figure 3.5b. We observe that P_{min} increases rapidly as $R_{pore}/R_{\mu gel}$ decreases. For experiments where $R_{pore}/R_{\mu gel}$ < ~0.4, the pressure required to detect an event is beyond the maximum pressure available in our current experiment (-500 mmHg). The steepness of the rise in P_{min} with decreasing $R_{pore}/R_{\mu gel}$ suggests the existence of minimum value for $R_{pore}/R_{\mu gel}$ for microgel translocation. Such a limit is determined by the properties of the microgel, such as internal density of charged groups, as well as chain flexibility and the strength of the solvent-polymer interactions. The trend in Figure 3.6a suggests that the translocation limit occurs at $R_{pore}/R_{\mu gel}$ ~0.4 for 570 nm radius pNIPAm-AAc microgels. We anticipate that this limiting value will be different for other types of soft particles.

For $R_{pore}/R_{\mu gel}$ larger than 1, no pressure is required in order for the microgels to translocate the pore; the electrophoretic force resulting from the applied voltage is capable driving microgel translocation. Finite-element simulation demonstrates that the electrophoretic force on the charged microgel from the 0.1 V between the two Ag/AgCl electrodes is sufficient to drive the translocation of particles that are smaller than the pore orifice. However, pressure-driven convective transport of the microgels is dominant at pressures greater than ~10 mmHg. Under this limiting condition, event rates can be predicted based on the pressure-dependent volumetric flow rate through the nanopore.[12,29] The dashed line in Figure 3.5 corresponds to predicted

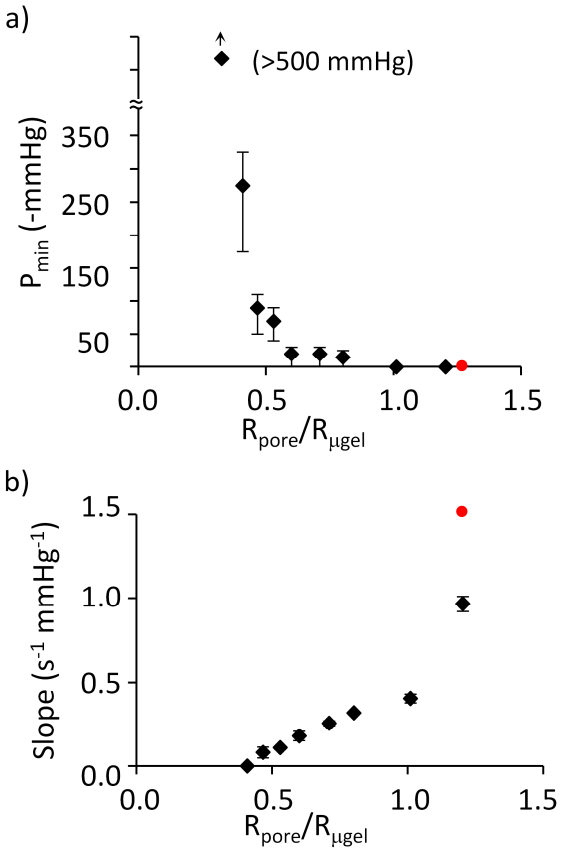

Figure 3.6 (a) Minimum pressure required to achieve translocation (P_{min}) for various $R_{pore}/R_{\mu gel}$. (b) Slopes of linear best fit lines to data contained in Figure 3.5 vs. $R_{pore}/R_{\mu gel}$. Best fit line was calculated using data where translocation events actually occurred. The red circles in (a) and (b) for $R_{pore}/R_{\mu gel}$ = 1.2 correspond to values based on the volumetric flow.

dependence of event rates on pressure for $R_{pore}/R_{\mu gel}$ = 1.2. The agreement with the experiment values for the same $R_{pore}/R_{\mu gel}$ is very good.

The slopes of the event rate vs. pressure plots ($s^{-1}mmHg^{-1}$) presented in Figure 3.5 are plotted in Figure 3.6b as a function of $R_{pore}/R_{\mu gel}$. The slopes represent the sensitivity of the event rate to the applied pressure. Above the minimum value of $R_{pore}/R_{\mu gel}$ ~ 0.4, the slopes increase gradually with increasing $R_{pore}/R_{\mu gel}$; a step increase in sensitivity occurs when $R_{pore}/R_{\mu gel}$ is greater 1. For $R_{pore}/R_{\mu gel} >> 1$, the event rate is determined by the volumetric flow carrying the particles through the pore. The dependence of event rate on pressure for $0.4 < R_{pore}/R_{\mu gel} < 1$ is complex, because the translocation of the microgel is hindered by their compression, which is a function of $R_{pore}/R_{\mu gel}$ and the applied pressure. The slowing down of the particles as they squeeze through the orifice reduces the volumetric flow through the pore (at applied constant pressure), reducing the observed event rate. Lower pressures and/or smaller pores result in longer translocation events (Fig 3.3), reducing the flow rate and lead to decreased event rates. However, once $R_{pore}/R_{\mu gel} > 1$, hindrance of the flow due to slow translocation is reduced and the slope of the event rate vs. pressure increases significantly, as shown in Figure 3.6b. For comparison, the pressure sensitivity of the event rate for $R_{pore}/R_{\mu gel}$ = 1.2, computed from the volumetric flow rate through the pore, is plotted in Figure 3.6b (red circle). The difference in the experimental and predicted values, albeit small, may arise from the Coulombic repulsion between the negative surface charge of the glass nanopore membrane and the negative charge of the microgel.

3.4 Conclusions

We have used the resistive pulse method to observe dynamics of the deformation of 570 ± 50 nm radius pNIPAm-AAc microgels as they are driven through a small conical pore embedded in a glass membrane. Our results show that both deformation and compression of the microgel occurs during translocation, resulting in the expulsion of its interior solution and a change in microgel conductivity. A minimum nanopore-to-microgel radius ratio of ~0.4 is observed for translocation, suggesting a theoretical limit imposed by the compressibility of the microgel and Columbic repulsion with the pore walls. This value is likely to depend on the particle and pore properties such as charge and particle polymer composition.

The ability of microgel to squeeze through pores of smaller diameter illustrates the soft, flexible nature of the particle as well as the importance of considering a particle's mechanical flexibility in designing synthetic nanoparticles, such as those used in drug delivery systems Resistive pulse methods, such as those described here, are likely to provide significant and fundamental insights into microgel compressibility and the ability of soft particles to translocate through complex biological matrices.

3.5 References

(1) Holden, D. A.; Hendrickson, G. R.; Lan, W.-J.; Lyon, L. A.; White, H. S. *Soft Matter*, **2011**, 7, 8035-8040.

(1) Mitragotri, S.; Lahann, J. *Nat. Mater*., **2009**, 8, 15-23.

(2) Nel, A. E.; Madler, L.; Velogol, D.; Xia, T.; Hoek, E. M. V.; Somasundaran, P.; Klaessig, F.; Castranova, V.; Thompson, M. *Nat. Mater*., **2009**, 8, 543-557.

(3) Gelperina, S. *Drugs and the Pharmaceutical Sciences*, **2006**, 159, 273-318.

(4) Illum, L.; Khan, M. A.; Mak, E.; Davis, S. S. *Int. J. of Pharmaceutics*, **1986**, 30, 17-28.

(5) Arinda, M.; Ghandehari, H. *J. of App. Toxicology*, **2010**, 30, 212-217.

(6) Nel, A.; Xia, T.; Madler, L.; Li, N. *Science*, **2006**, 211, 622-627.

(7) Elder, A.; Vidyasagar, S.; De Louise, L. *Nanomedicine and Nanobiotechnology*, **2009**, 1, 434-450.

(8) Hendrickson, G. R.; Lyon, L. A. *Angew. Chem. Int. Ed*., **2010**, 49, 2193-2197

(9) Holden, D. A.; Hendrickson, G. R.; Lyon, L. A.; White, H. S. *J. Phys. Chem. C*., **2011,** *115,* 2999–3004.

(10) Coulter, W. H. US Patent No. 2656508. Oct. 20, 1953.

(11) Henriquez, R. R.; Ito, R.; Sun, L.; Crooks, R. M. *Analyst*, **2004**, 129, 478-482.

(12) Lan, W.-J.; Holden, D. A.; Zhang, B.; White, H. S. *Anal. Chem*., **2011**, *83* (10), 3840–3847.

(13) Baley, H.; Martin, C. R., *Chem. Rev*., **2000**, 100, 2575-2594.

(14) Choi, Y.; Baker, L. A.; Hillebrenner, H.; Martin, C. R. *Phys. Chem. Chem. Phys*., **2006**, 8, 4976-4988.

(15) Harrell, C. C.; Choi, Y.; Horne, L. P.; Baker, L. A.; Siwy, Z. S.; Martin, C. R. *Langmuir*, **2006**, 22, 10837-10843.

(16) Ito, T.; Sun, L.; Bevan, M.; Crooks, R. M. *Langmuir*, **2004**, 20, 6940-6945.

(17) Petrossian, L.; Wilk, S. J.; Joshi, P.; Goodnick, S. M.; Thornton, T. J. *J. Phys. Conf. Ser*., **2008**, 109, 012028.

(18) Lee, S.; Zhang, Y.; Harrell, C. C.; Martin, C. R.; White, H. S. *Anal. Chem*., **2004**, 76, 6108-6115.

(19) Giehart, B. C.; Howitt, D. G.; Chen, S. J.; Zhu, Z.; Kotecki, D. E.; Smith, R. L.; Collins, S. D. *Sens. Actuators B*, **2008**, 132, 593-600.

(20) Fologea, D.; Gershow, M.; Ledden, B.; McNabb, D. S.; Golovchenko, J. A.; Li, J. *Nano Lett*., **2005**, 5, 1905.

(21) Han, A.; Schurmann, G.; Mondin, G.; Bitterli, R. A.; Hagelbach, N. G.; de Rooij, N. F.; Staufer, U. *Appl. Phys. Lett*., **2006**, 88, 093901.

(22) Sexton, L. T.; Mukaibo, H.; Katira, P.; Hess, H.; Sherrill, S. A.; Horne, L. P.; Martin, C. R. *J. Am. Chem. Soc*., **2010**, 132, 6755-6763.

(23) Deamer, D. W.; Branton, D. *Acc. Chem. Res*., **2002**, 35, 6755-6763.

(24) Baley, H. *Curr. Opin. Chem. Biol*., **2006**, 10, 628-637.

(25) Ying, Y.-L.; Wang, H.-Y.; Sutherland, T. C.; Long, Y.-T. *Small*, **2011**, 7, 87-94.

(26) Pelton, R. *Adv. Colloid Interface Sci*., **2000**, 85, 1-33.

(27) Hoare, T.; Pelton, R., *Langmuir* **2004**, 20 (6), 2123-2133

(28) Zhang, B.; Galusha, J.; Shiozawa, P. G.; Wang, G.; Bergren, A. J.; Jones, R. M.; White, R. J.; Ervin, E. N.; Cauley, C. C.; White, H. S. *Anal. Chem*., **2007**, 79, 4778-4787.

(29) Lan, W.-J.; White, H. S. *J. Phys. Chem. C*., **2011**, 115(8) 18445-18452.

(30) Kim, J.; Serpe, M. J.; Lyon, L. A. *Angew. Chem. Int. Ed*., **2005**, 44, 1333-1336.

(31) Suarez, I. J.; Fernandez-Nieves, A.; Marquez, M. *J. Phys. Chem. B*., **2006**, 110, 25729-25733.

CHAPTER 4

RESISTIVE-PULSE DETECTION OF MULTILAMELLAR LIPOSOMES

4.1 Introduction

In this chapter, we report investigations of the translocation behavior of 190 to 450 nm radius multilamellar liposomes through a single conical nanopore embedded in a glass membrane.[1] Translocation of biological particles, such as liposomes, through porous materials is of great interest due to the important role that these particles play in both the scientific and medical communities, particularly in drug delivery systems[2,3] and treatment of diseases.[4,5] The liposome structure is well documented,[6-8] comprising of a hydrophilic, aqueous filled interior surrounded by a thin hydrophobic lipid bilayer. Multilamellar liposomes contain concentric, repeating bilayers providing the liposome the ability to transport both hydrophobic and hydrophilic molecules. Once in contact with a cell membrane, a liposome may fuse with the membrane releasing its contents into the cell.[6] For example, lymphomatous meningitis has been commercially treated by liposomal delivery of a chemotherapeutic agent to the targeted cells.[9] Yet, despite their potential applications, the full extent of how liposomes pass through biological porous materials is still unclear. Herein, we demonstrate the ability to directly measure the translocation of a multilamellar

liposome through a single conical nanopore under biologically relevant pressures by means of a resistive-pulse technique.

The resistive-pulse method has been used for decades to monitor the translocation of various particles and molecules through a constriction zone.[10-13] For example, in 1977 DeBlois reported on the size determination of a 60 nm diameter virus.[14] In the resistive-pulse method, particle translocation is monitored by applying a potential across the electrolyte filled pore and measuring the ionic current generated through the pore.[15,16] As a particle translocates the pore, it displaces the electrolyte solution in the pore, decreasing the electrolyte flux and the current. The current is measured as a function of time and can be analyzed to determined particle concentration, charge, shape, size, as well as chemical and physical interactions with the pore.[14,17-30] We recently reported an investigation of the translocation dynamics of flexible, hydrated *N*-isopropyl-*co*-acrylic acid microgels through nanopores. In those experiments the translocation of microgels through pores of dimensions smaller than the pore itself require both deformation and dehydration of the microgel, giving information into the translocation of flexible, soft particles through a porous material.[31,32] In this report, we demonstrate that liposomes can be detected by the resistive-pulse method, providing insight into the liposome flexibility as it passes through a nanopore. The temperature dependence of the liposome translocation, below and above the lipid bilayer transition temperature, is reported.

4.2 Methods and Materials

4.2.1 Chemicals

K_2HPO_4, KH_2PO_4, KCl, chloroform, and anhydrous methanol were obtained from Mallinckrodt Chemicals and were used without further purification. Water (>18 MΩ·cm) was obtained from a Barnstead E-Pure water purification system. Trimethylchlorosilane was purchased from Gelest, Inc. (Morrisville, PA) and used without further purification. 1,2-dipalmitoyl-*sn*-glycero-3-phosphocholine (DPPC), 1,2-dilauroyl-*sn*-glycero-3-phosphocholine (DLPC), 1,2-dipalmitoyl-*sn*-glycero-3-phospho-(1'-*rac*-glycerol) (sodium salt) (DPPG), and 1,2-dioleoyl-*sn*-glycero-3-phospho-L-serine (sodium salt) (DOPS) phospholipids were obtained from Avanti Polar Lipids, Inc (Alabaster, AL) and stored at -80 ℃.

4.2.2 Preparation of Liposomes

A standard extrusion technique was used to prepare multilamellar liposomes with radii between 190 and 450 nm. The phospholipids used for liposome preparation were mixed prior to extrusion by adding 0 – 9% (mol/mol) (0 – 0.15 mg) DPPG or DOPS, dissolved in a solution of 1:3 methanol-chloroform, to a 1 mL chloroform solution containing 1 mg DPPC or DLPC, respectively. DPPG was added to DPPC while DOPS was added to DLPC due to their similar transition temperatures: T_c(DPPG) = 41 ℃ vs. T_c(DPPC) = 41 ℃, and T_c(DOPS) = -11 ℃ vs. T_c(DLPC) = -1 ℃. Liposomes comprising pure DPPC or DLPC were only dissolved in chloroform. Chloroform and methanol were removed under N_2 until visibly dry. Trace amounts of chloroform were removed by placing the lipid mixture under vacuum for 3-5 h. at room

temperature. After vacuum, dried lipids were immediately rehydrated above the transition temperature (> 41 ℃ for DPPG/DPPC and > -1 ℃ for DOPS/DLPC) in 1 mL pure water (>18 MΩ·cm) for 1-2 h. with occasional light shaking. Liposomes were formed from the lipid-water solution by the forcing the mixture through either a 0.8 μm or 1.0 μm diameter Nucleopore Track-Etch Membrane (Whatman) a minimum of 15 times.

Liposomes were sized using dynamic light scattering (DLS) technique with a NiComp 380 ZLS Zeta Potential Analyzer (Particle Sizing Systems). DLS indicated that the liposomes used in this study have a large size distribution (10 – 45%) (see Table 4.1). Aqueous solutions containing between ~1 x 10^8 and ~1 x 10^{10} liposomes/mL and 25 mM KCl, buffered at pH 7.0 with 2.5 mM K_2HPO_4 / KH_2PO_4, were used in translocation experiments. As the exact structure of the multilamellar liposomes is unknown, concentrations were estimated by assuming complete conversion from lipid solution to unilameller liposomes, with an average phospholipid surface area of 62.9 $Å^2$/lipid molecule,[33-34] and the radius determined by DLS measurements.

4.2.3 Translocation Experiments

Translocation experiments were performed using glass nanopore membranes (GNMs), consisting of a single conical pore embedded at the end of sealed glass capillary. A schematic diagram of the setup is shown in Figure 4.1. Fabrication of the GNM is described elsewhere in detail.[13] The small orifice radii of the nanopores used in this study ranged from 100 nm to 575 nm (± 10%), as determined by conductance measurements in a 1 M KCl solution.[13] Prior to

Table 4.1 Liposomes were prepared using a standard extrusion technique, as described in the main text, by passing a 1 mg/mL lipid solution in pure water through a Nuclepore track-etched polycarbonate porous membrane (Whatman) above the lipid bilayer transition temperature a minimum of 15 times. Extrusion of DPPG/DPPC or DOPS/DLPC lipid mixtures yielded liposomes with radii ranging from 192 nm to 447 nm with a dispersion of 5 to 20% (σ corresponds to 1 standard deviation). Sizes and standard deviations were determined by dynamic light scattering with a NiComp 380 ZLS Zeta Potential Analyzer set in vesicle sizing mode.

DLS Data		
Radius (nm)	σ (nm)	Lipid Type
192	34	DPPG/DPPC (5% DPPG)
198	40	DOPS/DLPC (5% DOPS)
203	38	DPPG/DPPC (9% DPPG)
367	79	DPPG/DPPC (5% DPPG)
389	40	DLPC
447	23	DPPC

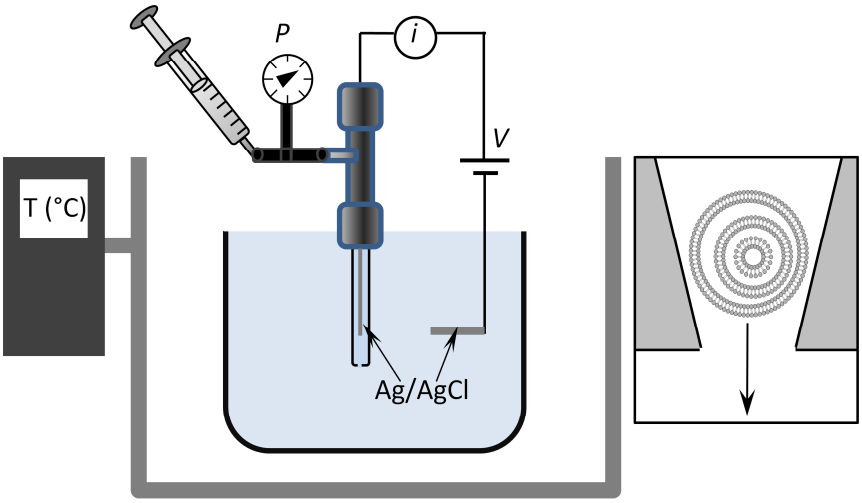

Figure 4.1 Schematic of the experimental setup for detecting liposome translocation through a nanopore embedded in the end of a glass capillary. The capillary was filled with and immersed in a 25 mM KCl electrolyte solution. Pressure is applied with a gas tight syringe attached to the interior of the capillary, while a voltage is applied between the two Ag/AgCl electrodes. The solution, membrane, and capillary are placed in a temperature-controlled vessel.

translocation experiments the GNM was rinsed in a 0.1 M nitric acid solution for 10 min., rinsed with H_2O, then soaked in a 2% (v/v) trimethylchlorosilane in acetonitrile overnight to reduce the negative surface charge, followed by a thorough rinsing with ethanol and water. Internal and external solutions, separated by the GNM, were filled with a solution of 25 mM KCl, buffered at pH 7.0 with 2.5 mM K_2HPO_4/KH_2PO_4, while the internal solution additionally contained the dispersed liposomes. A current was generated through the pore by applying a -0.1 V (internal vs. external) bias between two Ag/AgCl reference electrodes on opposing sides of the membrane; the current was monitored with a Dagan Cornerstone Series Chem-Clamp voltmeter/amperometer employing a high sensitivity pre-amplifier (0.05 to 10 nA/V) and a 10 kHz low-pass Bessel filter. Liposomes were driven across the membrane by convective flow generated by applying a positive pressure to the interior of the capillary with a gas tight syringe; the pressure was monitored with a Traceable Pressure Meter (Fisher Scientific). The amperometer was interfaced to a PC with a BNC 2090 or 2110 Board (National Instruments) and a PCI 6251 DAQ card (National Instruments). Data was recorded at 150 kHz, using in-house virtual instrumentation written in LabVIEW 8.6 (National Instruments). The temperature was controlled and monitored by placing the pore, buffer solution, and liposomes in a temperature controlled unit (Electronic BioSciences).

4.3 Results and Discussion

4.3.1 Translocation of Rigid Liposomes

Liposome translocation through the GNM was monitored and recorded as a function of time and temperature. Figure 4.2 shows a typical current-time (*i-t*) trace, normalized to the baseline current, for the translocation of 192 ± 34 nm radius multilamellar DPPG/DPPC (5%/95%) liposomes through a 340 ± 35 nm radius nanopore at a liposome concentration of ~3 x 10^8 liposomes/mL, at room temperature (23 ℃) and an applied pressure of +50 mm Hg (internal vs. external). This uninhibited liposome translocation is similar to that previously reported using polystyrene particles.[19,23] Translocation events, as shown by the resistive peaks in the *i-t* trace (Figure 4.2b), are present only when pressure is applied to the system, indicating that the applied voltage of -0.1 V (internal vs. external) is insufficient to drive the liposomes through the nanopore (data not presented).

The asymmetrical triangular shape in the *i-t* trace (Figure 4.2c) is characteristic of the electrolyte displacement by the liposome within the sensing zone during translocation from the interior to the exterior solution. As the liposome approaches the pore orifice from the conical side it displaces an increasing portion of the electrolyte solution in the pore's sensing zone, gradually decreasing the current. As the liposome passes out of the pore, the current rapidly increases back to its original level. In all experiments, translocation events correspond to liposomes passing from the internal solution of the capillary to the bulk solution.

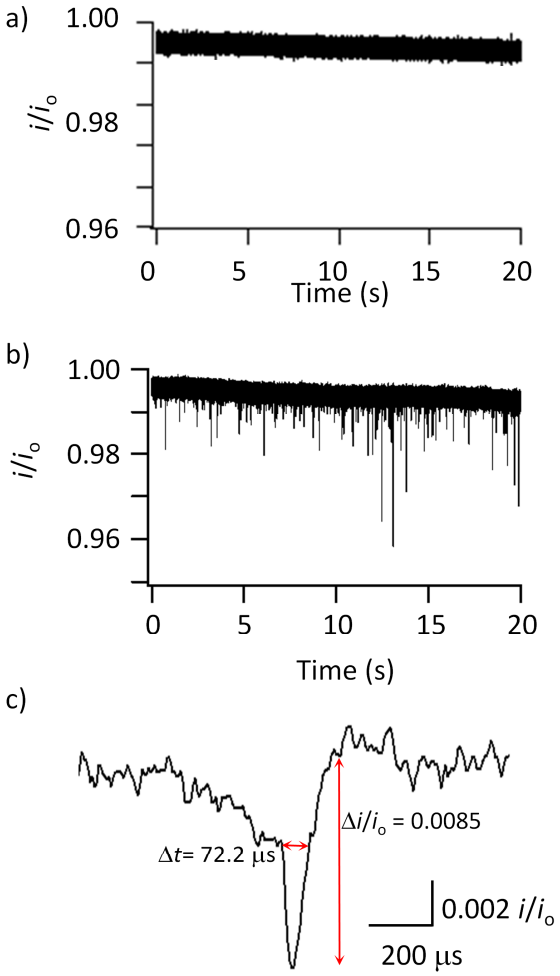

Figure 4.2 (a) Background *i-t* trace showing the open-pore current through a 340 ± 35 nm radius nanopore at a pressure, voltage, and temperature of +50 mmHg, -0.1 *V*, and 23 ℃, respectively. The current is normalize d to the largest current in the *i-t* trace. A slight drift in the current occurs due to a small drift in the potential of the Ag/AgCl electrodes. (b) *i-t* trace showing the translocation of 192 ± 34 nm radius DPPG/DPPC (T_c = 41 ℃) liposomes through the same pore at a concentration of ~3 x 10^8 liposomes/mL. (c) *i-t* trace of a single translocation event from (b). The translocation time (Δt) and the normalized current decrease ($\Delta i/i_o$) are indicated on the figure.

Translocation events for liposomes are characterized by their translocation time (Δt), measured as the width of the translocation peak at half its maximum height, as well as the maximum decrease in current normalized to the baseline current ($\Delta i/i_o$). Figure 4.2c shows a typical *i-t* trace of a single uninhibited translocation event and the values for Δt and $\Delta i/i_o$ of 72.2 μs and 0.0085, respectively. The average values of Δt and $\Delta i/i_o$ (N = 150 events) for the translocation of the 192 ± 34 nm radius multilamellar liposomes through a pore with radius of 340 ± 35 nm are 82 ± 24 μs and 0.005 ± 0.003, respectively. A plot of $\Delta i/i_o$ vs. Δt and individual histograms of Δt and $\Delta i/i_o$ for the translocation events through the 340 ± 35 nm pore are shown in Figure 4.3. In agreement with size distribution data obtained from DLS measurements (Table 4.1), the distributions of Δt and $\Delta i/i_o$ in these experiments are relatively large (Figure 4.2b) in comparison to previous results using polystyrene particles[19] or microgels,[31,32] where uniform size distributions lead to uniform Δt and $\Delta i/i_o$ values. However, Δt and $\Delta i/i_o$ are herein used to determine the extent of blockage and degree of interaction between the liposome and nanopore. Longer Δt and larger $\Delta i/i_o$ represent larger interactions and more complete blockages, while shorter Δt and smaller $\Delta i/i_o$ represent translocation events with little or no interaction with the pore, e.g. liposomes much smaller than the pore.

For temperatures below the lipid bilayer transition temperature, T_c, translocation behavior is expected to be a function of the pore size relative to the liposome size. Figure 4.4 shows the event rate for translocation of the 192 ± 34 nm radius DPPG/DPPC liposomes as a function of the pore radius, at a constant

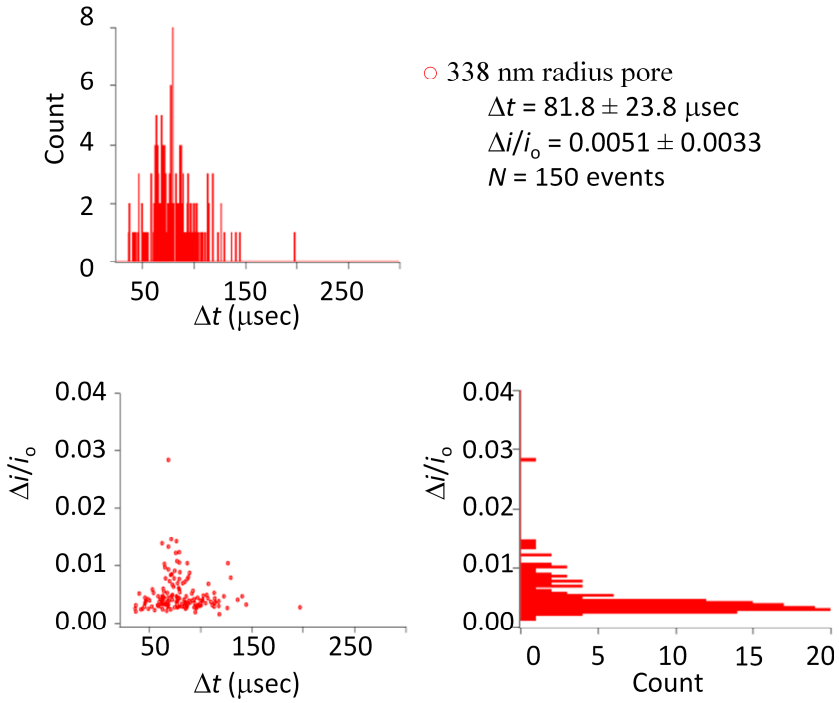

Figure 4.3 A plot of $\Delta i/i_o$ vs. Δt for translocation of 192 ± 34 nm radius liposomes (5% DPPG/95% DPPC) through a 340 ± 35 nm radius nanopore is shown in the lower left hand corner. Histograms of Δt and $\Delta i/i_o$ for the same data set are shown in above and to the right, respectively. In this experiment, the applied pressure was +50 mmHg and the voltage was -0.1 *V*. The spread in $\Delta i/i_o$ (64%) agrees well with the liposome volume distribution (53% based on the volumes of the 192 ± 32 nm radius liposomes). The deviation in Δt (29%) is smaller, reflecting the dependence of Δt on particle radius, rather than volume.

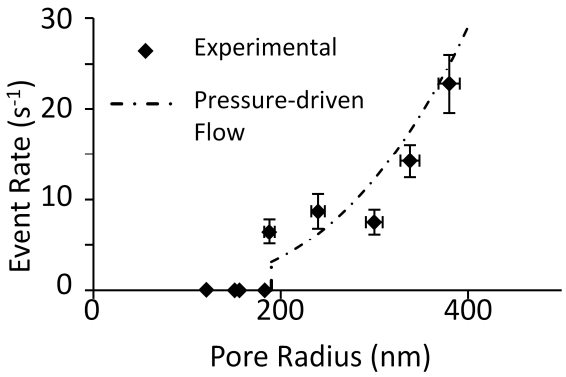

Figure 4.4 A plot of the event rate vs. pore size for the translocation of 192 ± 34 nm radius DPPG/DPPC (T_c = 41 ℃) liposomes at a concentration of ~3 x 10^8 liposomes/mL. The pressure, voltage and temperature were 50 mmHg, -0.1V and 23 ℃. Dashed line represents the theoretical e vent rate based on calculated pressure-driven volumetric flow rates through the nanopore above the liposome radius. No translocation was observed when the pore radius was smaller than the liposome radius.

concentration of ~3 x 10^8 liposomes/mL, pressure of +50 mmHg (internal vs. external) and temperature of 23 ℃ ($T < T_c$ = 41 ℃). For pore sizes larger than the particle, translocation occurs as described above and is in good agreement with pressure-driven flow theory developed by Lan et al. and described by equation 4.1.[19,26]

$$E.R. = \frac{3\pi r^3 P}{8\eta \cot(\theta)} C \qquad (4.1)$$

where *E.R.* is the event rate, *r* is the radius of the nanopore, *P* is the applied pressure, η is the solution viscosity, θ is the half cone angle of the nanopore, and *C* is the concentration of the nanoparticles.

Additionally, for pores with dimensions smaller than the liposome, translocation does not occur due to the relative inflexibility of the liposomes at temperatures below T_c.[6] Attempted translocation events led to stable current blockages (~25%) for extended durations, during which the pressure was not observed to change (± 2 mmHg). These blockages were only reversible with a reverse in pressure (Figure 4.5).

4.3.2 Translocation of Soft Liposomes

Liposome translocation events at $T > T_c$ through pores with radii larger than the liposome were found to be similar to those described above for $T < T_c$. As shown in Figure 4.6, *i-t* traces demonstrate a similar decrease in current proportional to the volume of the sensing zone occupied by the liposome. In these experiments, the liposomes are not physically inhibited by the pore during

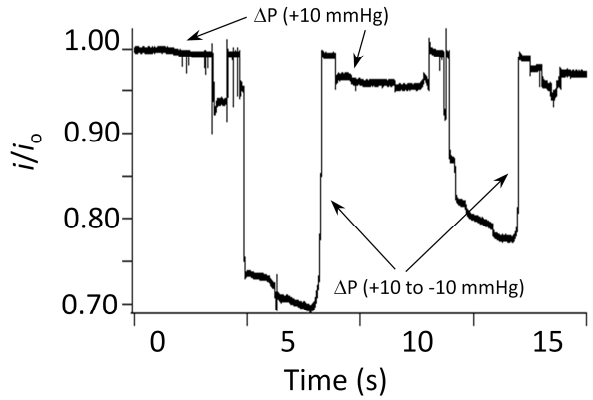

Figure 4.5 *i-t* trace corresponding to the capture and release of 367 ± 79 nm radius DPPG/DPPC liposomes in a 210 ± 20 nm nanopore. Liposomes were larger than the pore and below their transition temperature ($T < T_c$) making them incapable of deformation and translocation. Capture was achieved at a pressure of +10 mmHg, while release was achieved at -10 mmHg. The experiment was run at a voltage of -0.1 *V*, temperature of 23 ℃, in a solution containing 25 mM KCl, 2.5 mM K_2HPO_4/KH_2PO_4, at pH 7.0.

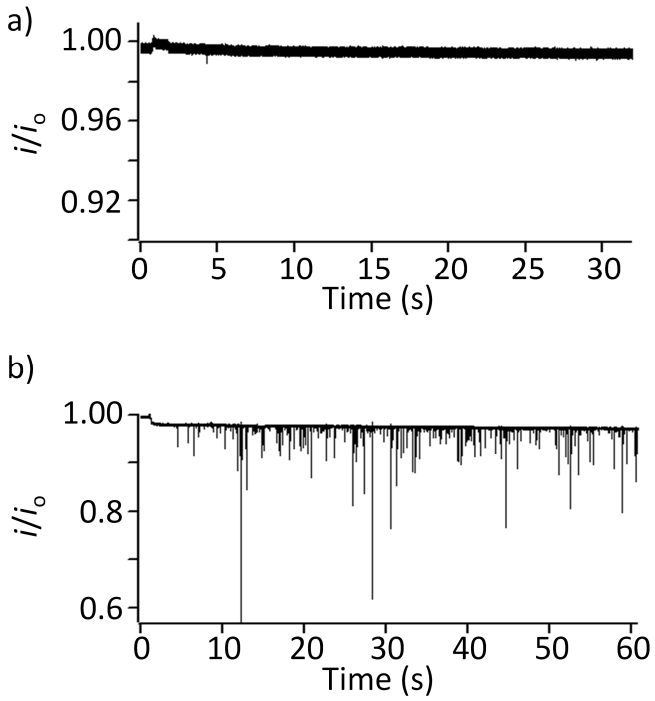

Figure 4.6 (a) *i-t* trace showing the open-pore current through a 492 nm radius nanopore at V = -0.1 *V*, T = 23 ℃, and P = +10 mmHg in a solution of 25 m M KCl, buffered at pH 7.0 with 2.5 mM K_2HPO_4/KH_2PO_4. (b) Translocation of 389 ± 40 nm DLPC (T_c = -1 ℃) liposomes under th e same conditions as in (a).

translocation and require no deformation; thus, translocation is similar, both in Δt and $\Delta i/i_o$, to events below the transition temperature. Δt and $\Delta i/i_o$ values obtained using the same nanopore (525 nm radius) were measured at 23 ℃ for liposomes of similar sizes (389 ± 40 nm vs. 367 ± 79 nm radius) but with different compositions (100% DLPC vs. 5% DPPG/95% DPPC, respectively) and transition temperatures (T_c = -1 ℃ vs. T_c = 41 ℃, respectively). The Δt and $\Delta i/i_o$ values for the liposomes when $T > T_c$ are 100 ± 33 μs and 0.019 ± 0.023, respectfully, while values of 102 ± 42 μs and 0.013 ± 0.011 were recorded for the liposomes when $T < T_c$ (Figure 4.7). These results verify that Δt and $\Delta i/i_o$ are unaffected by the physical state (solid-like vs. fluid-like) of the liposome where no deformation for passage is required.

Experiments were performed using pores of dimensions smaller than the liposomes at temperatures above T_c. These events demonstrate full translocation (Figure 4.8) in contrast to low blockage at low temperature (Figure 4.5). As previously explained, at elevated temperatures the lipid bilayers are in a fluid-like state[6] creating a liposome capable of deformation and translocating through smaller pores. When the pore size is only slightly smaller than the liposome, minimal deformation is required and the resulting *i-t* trace demonstrates characteristics similar to liposomes at $T < T_c$. For example, Figure 4.8a shows *i-t* traces for 389 ± 40 nm radius DLPC liposomes requiring minimal squeezing during translocation through a 318 nm radius pore with +10 mmHg pressure applied, while the inset shows a single typical *i-t* trace. However, if the pore size is decreased further (R_{pore} = 220 ± 20 nm, Figure 4.8b), the resulting *i-t* traces

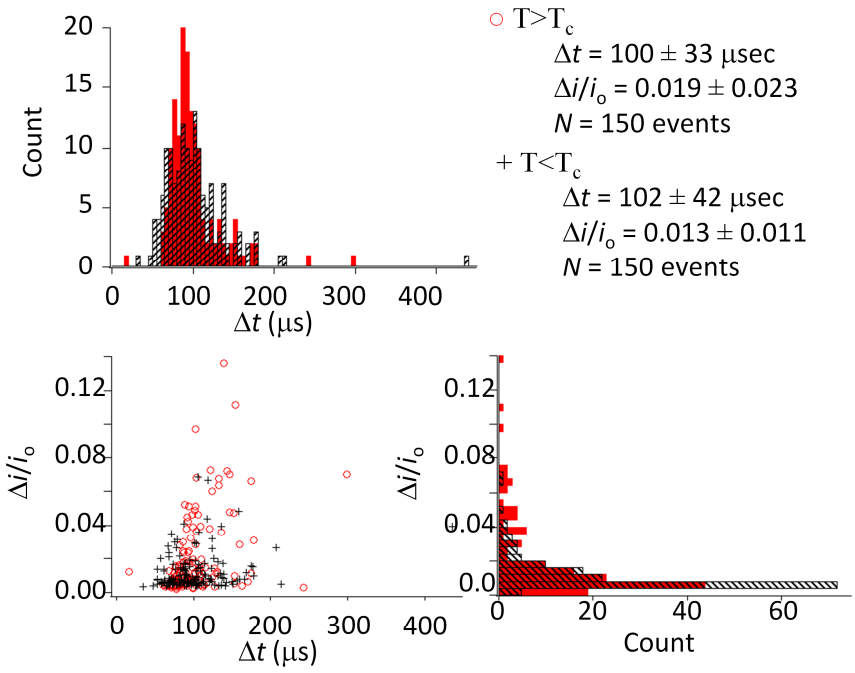

Figure 4.7 Plots showing $\Delta i/i_o$ vs. Δt and histograms of $\Delta i/i_o$ and Δt for translocation of DLPC (389 ± 40 nm radius) and DPPG/DPPC (367 ± 79 nm radius) liposomes through a 525 nm radius pore. The temperature, applied pressure, and voltage were 23 ℃, +10 mmHg, and -0.1 *V*, respectively. Due to their different transition temperatures, T_c(DLPC) = -1 ℃ and T_c(DPPG/DPPC) = 41 ℃, the DLPC liposomes were in a fluid-like state, while the DPPG/DPPC liposomes were in a solid-like state.

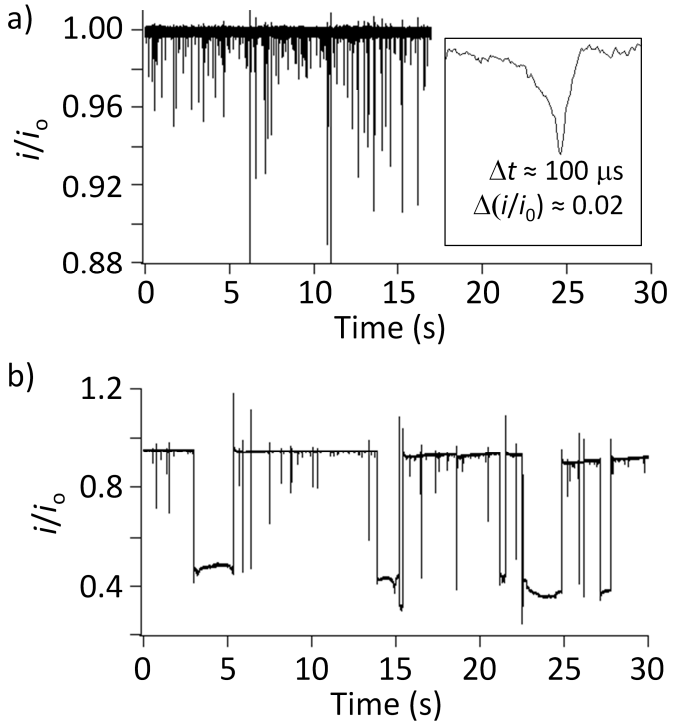

Figure 4.8 The translocation of 389 ± 40 DLPC (T_c = -1 ℃) liposomes though (a) 320 ± 30 nm and (b) 220 ± 20 nm radius nanopores at V = -0.1*V*, P = +10 mmHg and T = 23 ℃. Inset in (a) shows *i-t* trace for a single event.

became more rectangular with longer translocation times (Δt up to 10 s) and display larger current blockages ($\Delta i/i_o > 0.5$). The increases in Δt and $\Delta i/i_o$ are due to physical interactions of the liposome with the pore. $\Delta i/i_o$ values ~1 are possible, however due to imperfections in the GNM shape; a tight seal may not form allowing current to pass though the GNM at the same time as a blockage event.

The mechanism by which the liposome translocates the nanopore is believed to be similar to the extrusion process used to create the liposomes, where the lipid vesicle solution was pushed under pressure and at elevated temperatures through a porous membrane. Similar to the extrusion process, we speculate that the liposome is stripped of excess lipid as it translocates and is resized to the dimensions of the nanopore. However, the concentration of liposomes in the external receiving solution is insufficient to re-measure the liposome sizes using conventional techniques.

4.3.3 Liposome Phase Transition

Studies demonstrating the ability of the liposome to squeeze through a nanopore smaller than itself were performed while continuously varying the experimental temperature, as shown in Figure 4.9. 367 ± 79 nm radius (5% DPPG / 95% DPPC, T_c = 41 ℃) liposomes were placed in the interior capillary solution at a concentration of ~5 x 10^9 liposomes/mL. A voltage of -0.1 V was applied to monitor their translocation through a 210 ± 20 nm radius nanopore, while a pressure of +10 mmHg was applied to drive the liposomes through the pore and into the exterior solution. The temperature was initially set at 55 ℃ and then decreased at 2 ℃ intervals every 30-60 sec (Figure 4.9a). Once the

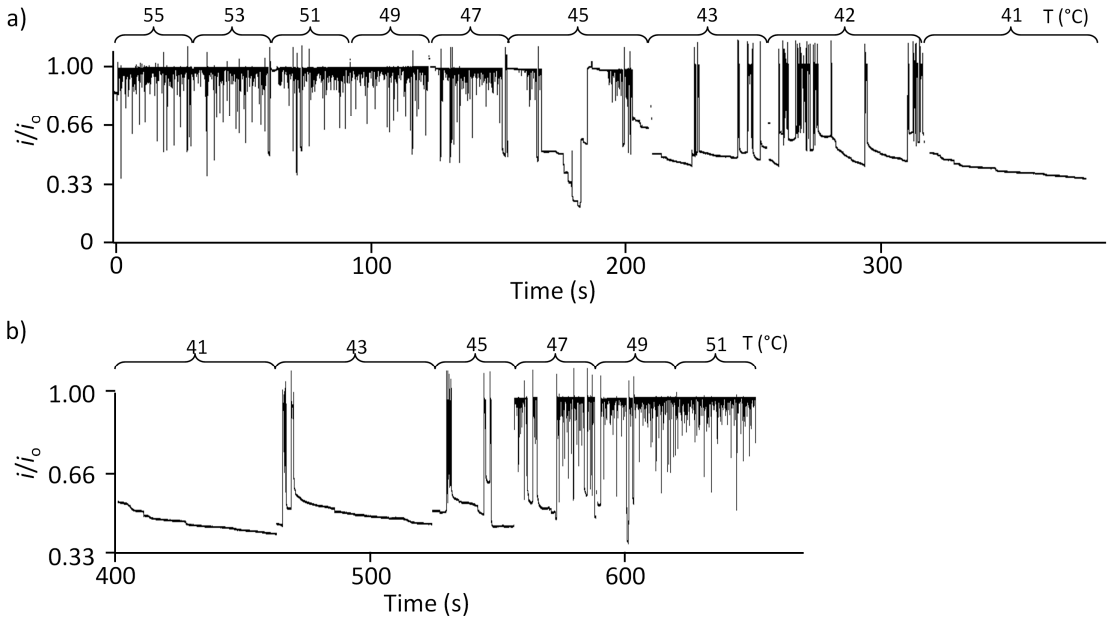

Figure 4.9 Translocation of 367 ± 79 nm radius DPPG/DPPC (T_c = 41 ℃) liposomes through a 210 ± 20 nm radius nanopore at a concentration of ~5 x 10^9 liposomes/mL, V = -0.1 *V*, and P = +10 mmHg. Temperature was (a) decreased continuously from 55 ℃ to 41 ℃ at 2 ℃ increments , then (b) increased back to 51 ℃.

temperature reached the liposome T_c, the temperature was raised by 2 ℃ until a final temperature of 51 ℃ was achieved (Figure 4.9b). At high temperatures, where the lipid membrane is highly flexible, deformation and translocation of the liposome occurs in agreement with previous results. When the temperature is decreased to values close to the transition temperature, the peaks become more rectangular shaped, deeper, and wider due to the difficulty of the liposome has in deforming and passing through the pore orifice. When the temperature reached the liposome's transition temperature at 41 ℃, the pulses became increasingly long, eventually lasting indefinitely due to the solid-like liposome not being able to pass through the nanopore. As the temperature was increased again, the rigid, pore-blocking liposome reverts to its more fluid-like state and is able to pass through the pore.

Figure 4.10 shows the average translocation time (defined as the average time occupied with $\Delta i/i_o > 0.5$) as a function of the temperature. Blockages with short duration times occur at temperatures significantly above the transition temperature, while longer blockages occur when the experimental temperature approaches the lipid transition temperature. For instance, Δt_{ave} increases from hundreds of microseconds (~100 μs at 55 ℃) to a few seconds (~1 – 4 s at 42 ℃) and then to more than 120 s at 41 ℃ (the maximum run time of these experiments), in agreement with expectations based on the structure of the lipid bilayer, where above its transition temperature it is in a flexible, fluid-like state capable of deforming and translocating, while below the T_c it is rigid and blocks the pore.

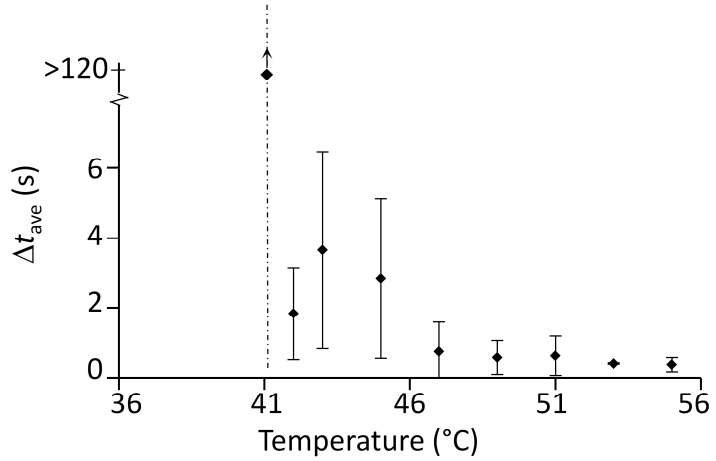

Figure 4.10 The average translocation time from *i-t* traces shown in Figure 4.9 as a function of the temperature. At $T < T_c$, the solid-like liposomes are not able to translocate, and thus block the pore orifice for an indefinite period. Dashed line represents the transition temperature of the DPPC/DPPG lipid used in this experiment.

4.4 Conclusions

We have demonstrated that translocation of water-filled multilamellar liposomes through an individual nanopore can be detected and analyzed using the resistive-pulse method. Additionally, these experiments provide insight into the deformation of liposomes during translocation through rigid pores at temperatures both above and below their transition temperature. This research and our previous studies of polymer microgel translocation, demonstrates the potential applications of using the resistive-pulse method to quantitatively study the mechanism and dynamic processes of soft particle translocation through porous materials.

4.5 References

(1) Holden, D. A.; Watkins, J. J.; White, H. S. *Langmuir* **2012**, 28, 7572-7577.

(2) Kulkarni, P. R.; Yadav, J. D.; Vaidya, K. A. *Int. J. Curr. Pharm. Res*. **2011**, *2*, 10-18.

(3) Alsarra, I. A.; Hamed, A. Y.; Alanazi, F. K. *Neuromethods* **2010**, *45*, 175-203.

(4) Tran, M. A.; Watts, R. J.; Robertson, G. P. *Pigment Cell & Melanoma Res*. **2009**, *22*, 388-399.

(5) Maeda, H.; Bharate, G. Y.; Daruwalla, J. *Eur. J. Pharm. Biopharm*. **2009**, 71, 409-419.

(6) New, R. R. C. *Liposomes: a practical approach*. Oxford University Press: New York, 1990

(7) Phillippot, J. R.; Schuber, F., *Liposomes as tools in basic research and industry*. Boca Raton: CRC Press, 1995.

(8) Lasic, D. D.; Papahadjopoulos, D., *Medical applications of liposomes*, New York: Elsevier, 1998.

(9) Pacira Pharmaceuticals, Inc. 10450 Science Center Drive San Diego, CA 92121, (858) 625 2424.

(10) Coulter, W. H. U. S. Patent no. 2656508, Oct. 20, 1953.

(11) Bayley, H.; Martin, C. R. *Chem. Rev*. **2000**, *100*, 2575-2594.

(12) Lines, R. W. In *Particle Size Analysis*; Stanley-Wood, N. G., Lines, R. W., Eds; Royal Society of Chemistry: Cambridge, U.K., 1992.

(13) Zhang, B.; Galusha, J.; Shiozawa, P. G.; Wang, G.; Bergren, A. J.; Jones, R. M.; White, R. J.; Ervin, E. N.; Cauley, C. C.; White H. S. *Anal. Chem*. 2007, **79**, 4778-4787.

(14) DeBlois, R. W.; Wesley, R. K. A. *J. Virol.* **1977**, *23*, 227-233.

(15) Ho, C.; Qiao, R.; Heng, J. B.; Chatterjee, A.; Timp, R.J.; Aluru N. R.; Timp, G. *Proc. Natl. Acad. Sci. U.S.A.* **2005**, *102*, 10445.

(16) Li, N.; Yu, S.; Harrell, C.; Martin, C. R. *Anal. Chem.* **2004**, *76*, 2025.

(17) Murray, R. W. *Chem. Rev.* **2008**, *108*, 2688-2720.

(18) Sun, L; Crooks, R. M. *J. Am. Chem. Soc.* **2000**, *122*, 12340-12345.

(19) Lan, W.-J.; Holden, D. A, Zhang, B.; White, H. S. *Anal. Chem.* **2011**, *83*, 3840-3847.

(20) Ito, T.; Sun, L.; Crooks, R. M. *Anal. Chem*. **2003**, *75*, 2399-2406.

(21) Ito, R.; Sun, L.; Bevan, M. A.; Crooks, R. M. *Langmuir* **2004**, *20*, 6940-6945.

(22) Henriquez, R. R.; Ito, T.; Sun, L.; Crooks, R. M. *Analyst* **2004**, *129*, 478-482.

(23) DeBlois, R. W.; Bean, C. P. *Rev. Sci. Instrum*. **1970**, *41*, 909-906.

(24) Petrossian, L.; Wilk, S. J.; Joshi, P.; Goodnick, S. M.; Thornton, T. J. *J. Phys.: Conf. Ser.* **2008**, *109*, 012028.

(25) Zhang, B.; Wood, M.; Lee, H. *Anal. Chem.* **2009**, *81*, 5541-5548.

(26) Lan, W.-J.; Holden, D. A.; Liu, J.; White, H. S. *J. Phys. Chem. C.* **2011**, *115*, 18445–18452.

(27) Kasianowicz, J. J.; Brandin, E.; Branton, D.; Deamer, D. W. *Proc. Natl. Acad. Sci. U.S.A.* **1996**, *93*, 13770-13773.

(28) Gu, L. Q.; Braha, O.; Conlan, S.; Cheley, S.; Baley, H. *Nature* **1999**, *398*, 686-690.

(29) Robertson, J. W. F.; Rodrigues, C. G.; Stanford, V. M.; Rubinson, K. A.; Krasilnikov, O. V.; Kasianowicz, J. J. *Proc. Natl. Acad. Sci. U.S.A* **2007**, *104*, 8207-8211.

(30) Reiner, J. E.; Kasianowicz, J. J.; Nablo, B. J.; Robertson, J. W. F. *Proc. Natl. Acad. Sci. U.S.A* **2010**, *107*, 12080-12085.

(31) Holden, D. A.; Hendrickson, G.; Lyon, L. A.; White, H. S. *J. Phys. Chem. C.* **2011**, *115*, 2999-3004.

(32) Holden, D. A.; Hendrickson, G.; Lyon, L. A.; Lan, W.-J., White, H. S. *Soft Matter* **2011**, *7*, 8035–8040

(33) Nagle, J. R.; Zhang, R.; Tristram-Nagle, S.; Sun, W.; Petrache, H.; Suter, R. M*. Biophys. J.* **1996**, *70*, 1419 - 1431.

(34) Feller, S. E.; Venable, R. M.; Pastor, R. W. *Langmuir* **1997**, *13*, 6555-6561.

CHAPTER 5

CONCLUSIONS

The results from experiments involving the translocation of soft, flexible nanoparticles through a rigid glass membrane using the resistive-pulse technique have been presented in this dissertation. The fundamental concepts and findings reported herein provide insight into the larger realm of research involving the dispersion of drug-carrying nanoparticles, particularly where kinetics and mechanics involved in membrane translocation processes are important.

In this dissertation two types of nanoparticles capable of delivering drugs, microgels and liposomes, were investigated. The resistive-pulse technique measures the change in conductivity of a nanopore as a particle passes through its orifice, resulting in a pulse which provides information about the physical and chemical properties of the nanoparticle.

The deformation and dehydration of 570 nm radius microgels during pressure-driven translocation through nanopores of dimensions smaller than the microgels were initially investigated and the results were reported in Chapters 2 and 3. This research has demonstrated that the resistive-pulse technique is capable of monitoring the dynamics of the deformation of individual particles as they pass through smaller pores, a process similar to biological processes such as cellular uptake, organ localization, extravasation into tumors, and excretion.

The insights gained from these experiments are critical to the work involved in developing new drug delivery vehicles, especially where the translocation of particles across biological membranes and through tight junctions is expected.

Investigations have shown that both a change in the physical structure as well as the conductivity occur during translocation where the microgel must pass through a significantly small pore. Furthermore, the compressibility, including both deformation and dehydration, of the microgel was determined, and is estimated to be about 40% of its original size. Consequently, the maximum particle size that will be able to penetrate a porous membrane at a given pressure can be extracted from these data and, along with other information gained in this study, used in the optimization of nanoparticles for drug-delivery systems.

In addition to monitoring the translocation of microgels, liposomes, also relevant to drug delivery applications, were analyzed and results were reported in Chapter 4. Liposomes made from DOPS/DLPC or DPPG/DPPC were fabricated between 190 and 450 nm radius and were chosen due to their ability to transition between rigid and flexible states by modifying the temperature. Translocation experiments have provided direct insight into the degree of rigidity of the liposome's structure, both above and below the lipid's bilayer transition temperature and through pores both larger and smaller than the particle. The real-time transition of the liposome from a flexible to a rigid structure is demonstrated and shows the importance of the physical and chemical structure of liposome when attempting translocation through small pores. These results

provide information useful to the development of vehicles for drug delivery into the human body where both temperature and flexibility are important.

Additionally, translocation event rates of particles through nanopores were analyzed using Poisson statistics and a method originally set forth by Davis and Giddings for separating chromatography peaks. In a stochastic process, events occur at random and a finite probability exists that two events will occur simultaneously and overlap. This research systematically developed this method for nanoparticle translocation through nanopores to determine the expected number of coincident or overlapping events. This analysis provides information regarding the expected number of peaks compared to the actual number of translocation events. Furthermore, deviations from these results suggest that the particles may not translocate at random and other forces must be considered such as adhesion, aggregation, and Coulombic forces.

In summary, this dissertation has presented results from fundamental studies on the translocation of microgels and liposomes through nanopores embedded in glass membranes. Both of these particles are relevant to the medical communities as transport vehicles for drug delivery systems in the human body, and various physical and chemical properties have been investigated including the flexibility, compressibility, and conductivity of the particles. The future applications of nanoparticles are continually expanding and this research provides some insights into the detection and analysis of soft, flexible nanoparticles for a variety of those applications.